UNIVERSITY OF NAPLES “FEDERICO II”

DOCTORATE

MOLECULAR MEDICINE AND MEDICAL BIOTECHNOLOGY

XXIX CYCLE

Molecular genetics and pathogenic mechanisms of hereditary anemias due to altered permeability of erythrocyte membrane

TUTOR

Prof. Achille Iolascon

CANDIDATE

Immacolata Andolfo

COORDINATOR

Prof. Vittorio Enrico Avvedimento

ACADEMIC YEAR

2015-2016

Table of contents

List of Abbreviations **1**

Abstract **2**

1. Background **4**

1.1 Red blood cell membrane: genesis, structure and function 4

1.2 Classification, diagnostic criteria and epidemiology of erythrocyte membrane defect-related anemias 6

1.3 Hereditary anemias due to RBC structural defects 7

1.3.1 Hereditary spherocytosis 7

1.3.2 Hereditary elliptocytosis and pyropoikilocytosis 11

1.3.3 Southeast Asian ovalocytosis 11

1.3.4 Other conditions 12

1.4 Anemias due to altered permeability of RBC membrane 13

1.4.1 Dehydrated hereditary stomatocytosis or xerocytosis 13

1.4.2 PIEZO1 15

1.4.3 KCNN4 16

1.4.4 Overhydrated hereditary stomatocytosis 18

1.4.5 Familial pseudohyperkalemia and cryohydrocytosis 18

1.4.6 ABCB6 19

1.5 Animal models of anemias due to RBCs defects 20

2. Aims of the study **23**

3. Materials and Methods **24**

3.1 Collection of all patients 24

3.2 FP patients 24

3.2.1 Whole exome sequencing (WES) of FP Irish family 24

3.2.2 Sanger sequencing analysis of ABCB6 gene 25

3.2.3 ABCB6 screening in donor blood subjects 25

3.2.4 Bioinformatic modeling of ABCB6 protein structure 25

3.2.5 Molecular cloning of ABCB6 and site-directed mutagenesis 26

3.2.6 Cell culture and transfection assay for ABCB6 26

3.2.7 Immunofluorescence analysis of ABCB6 27

3.2.8 Measurements of K+ fluxes in red blood cells of blood donor carrying ABCB6 R276W variant 27
3.2.9 Measurements of ouabain-plus-bumetanide-resistant Rb+ and K+ fluxes in ABCB6 transfected HEK-293 cells..... 27
3.2.10 RNA isolation, cDNA preparation and quantitative..... 28
3.2.11 Immunoblotting..... 28
3.2.12 Statistical analysis 28
3.3 DHS patients recruitment for the identification study of new causative gene/s..... 29
3.3.1 Whole exome sequencing and sequencing analysis of KCNN4. 29
3.3.2 Isolation and erythroid differentiation of CD34+ hematopoietic progenitor cells..... 29
3.3.3 K562 cell culture and erythroid differentiation 30
3.3.4 RNA isolation, cDNA preparation, and quantitative qRT-PCR..... 30
3.3.5 Red blood cell membrane preparation 30
3.3.6 Mouse embryo collection and Immunoblotting 31
3.3.7 Statistical analysis 31
3.4 DHS patients collection for PIEZO1 study 31
3.4.1 Direct sequencing of PIEZO1 31
3.4.2 Cloning, site direct mutagenesis and transfection assay..... 32
3.4.3 Measurements of ouabain-plus-bumetanide-resistant Rb+ and K+ fluxes in PIEZO1 transfected HEK-293 cells..... 32
3.4.4 Osmotic gradient ektacytometry 32

4. Results 33
4.1 Functional characterization of ABCB6 mutations in FP..... 33
4.1.1 Case Reports 33
4.1.2 ABCB6 mutational analysis in FP families and blood donor screening..... 34
4.1.3 ABCB6 mutations produce conformational changes in model structures 37
4.1.4 ABCB6 mutations cause no alteration of expression and cellular localization 39
4.1.5 ABCB6 mutation R276W increases potassium efflux from red blood cells of a blood donor 40
4.1.6 ABCB6 mutations cause cation flux alterations..... 42
4.2 KCNN4 gene identification as causative of DHS..... 43

4.2.1 Cases report 43
4.2.2 KCNN4 mutational analysis 44
4.2.3 Red cell membrane proteins in patients with KCNN4 mutations 46
4.2.4 KCNN4 during erythroid differentiation and mouse embryogenesis 47
4.3 Modifier effect of PIEZO1 variant on DHS phenotype 48
4.3.1 Cases report 48
4.3.2 Deformability analysis of RBCs of the families here analyzed 49
4.3.3 PIEZO1 mutational analysis 49
4.3.4 PIEZO1 expression analysis 50
4.3.5 Cation flux in PIEZO1 mutants 50

5. Discussion 52

6. Conclusions 57

7. References 58

9. List of publications related to the thesis 63

List of Abbreviations

AGLT, acidified glycerol lysis test
BM, bone marrow
CDA, congenital dyserythropoietic anemia
CHC, cryohydrocytosis
DHS, stomatocytosis
EMA, eosin-5-maleimide
ER, endoplasmic reticulum
FP, familial pseudohyperkalemia
Hb, hemoglobin
HDW, Hb distribution width
HE, hereditary elliptocytosis
HHA, hereditary hemolytic anemia
HPP, hereditary pyropoikilocytosis
HS, hereditary spherocytosis
HST, hereditary stomatocytosis
LDH, lactate dehydrogenase
MAF, minor allele frequency
MCHC, mean corpuscular Hb concentration
MCV, mean cell volume
NGS, next generation sequencing
OF, osmotic fragility
OHS, overhydrated hereditary stomatocytosis
OMIM, Online Mendelian Inheritance in Man
PBMC, peripheral blood mononuclear cell
PLT, platelet
qRT-PCR, quantitative RT-PCR
RBC, red blood cell
RDW, RBC distribution width
RhAG, Rh-associated glycoprotein
SAO, Southeast Asian ovalocytosis
SDS-PAGE, sodium dodecyl sulfate polyacrylamide gel electrophoresis
t-NGS, targeted-NGS
WB, western blotting
WES, whole-exome sequencing
αLELY, Low Expression Lyon
sTfR, soluble transferrin receptor

ABSTRACT

Genetic defects of erythrocyte transport proteins cause disorders of red blood cell volume that are characterized by abnormal permeability to the cation and, consequently, by changes in red cell hydration. Within this group of hereditary anemias we focused on familial pseudohyperkalemia and dehydrated hereditary stomatocytosis. The main aims of the project thesis are to study both the molecular genetics and the pathogenic mechanisms of these two disorders.

Isolated Familial Pseudohyperkalemia (FP) is a dominant red cell trait characterized by cold-induced 'passive leak' of red cell K+ into plasma. The causative gene of this condition is *ABCB6*, encoding an erythrocyte membrane ABC transporter protein bearing the Langereis blood group antigen system.

Dehydrated hereditary stomatocytosis (DHS) is an autosomal dominant congenital hemolytic anemia with moderate splenomegaly and often compensated hemolysis. Red cells are characterized by cation leak of the red cell membrane, reflected in elevated sodium content, decreased potassium content, elevated MCHC and MCV, and decreased osmotic fragility. The majority of symptomatic DHS cases reported to date have been associated with gain-of-function mutations in the mechanosensitive cation channel gene, *PIEZO1*.

Our study started with the recruitment of 97 patients affected by both FP and DHS from 41 unrelated families of Italian and foreign countries.

Regarding familial pseudohyperkalemia, analyzing three new families, we reported the first functional characterization of *ABCB6* mutants, including homozygous mutation V454A, heterozygous mutation R276W, and compound heterozygous mutations R276W and R723Q. All these mutations are annotated in public databases, suggesting that FP could be common in the general population. Indeed, we identified variant R276W in one of 327 random blood donors (0.3%). Measurement of cation flux demonstrated greater loss of K+ or Rb+ from HEK-293 cells expressing *ABCB6* mutants than from cells expressing ABCB6 WT. The R276W/R723Q mutations elicited greater cellular K+ efflux than did the other mutants tested.

Regarding dehydrated hereditary stomatocytosis by whole exome sequencing analysis of two previously undiagnosed DHS families we identified the second causative gene of DHS, the *KCNN4* gene, encoding the Gardos channel (KCa3.1), the erythroid Ca2+-sensitive K+ channel of intermediate conductance. We characterized the expression of *KCNN4* in the mutated patients and during erythroid differentiation of hematopoietic progenitor cell CD34+ and K562 cells. We

also analyzed *KCNN4* expression during mouse embryonic development. Finally, we demonstrated that the mutations in *KCNN4,* as for *PIEZO1*, cause a gain of function, by increasing potassium efflux.

Moreover, by analysing the genotype of the patients here collected, we characterized a new interesting mutation in *PIEZO1*, that is a duplication of two aminoacids localized in the pore of the channel, found in two families with different phenotype. We further analysed the modified effect of an additional *PIEZO1* missense variant carried by the family exhibiting the more severe phenotype. We found that the missense variant co-inherited with the duplication cause an augmented potassium efflux.

In conclusion, *ABCB6* missense mutations in FP erythrocytes show elevated K+ efflux. The patients are present at moderate frequency in the blood donor population. Storage of blood of these patients leads to significantly increased K+ levels, with serious clinical implications for neonates and infants receiving large-volume transfusions of whole blood. Genetic tests for FP could be added to blood donor pre-screening. Further study of ABCB6 function and trafficking could be informative for the study of other pathologies of red blood cell hydration.

The identification of *KCNN4* mutations in DHS patients supports recent studies that indicate it plays a critical role in normal erythrocyte deformation in the microcirculation and participates in maintenance of erythrocyte volume homeostasis. The characterization of *PIEZO1* and *KCNN4* mutations in DHS has contributed to the understanding of DHS pathogenesis that will be useful for the prognosis, the management, the follow-up, and the treatment of these patients.

1. Background

1.1 Red blood cell membrane: genesis, structure and function

During its long life span of 120 days, the red blood cell (RBC) is forced to cross the pores of splenic sinusoids thousands of times. This cell has an ongoing relationship with the spleen that contributes to remodeling during the first week of its life, participating in the passage from reticulocyte to erythrocyte. Moreover the spleen plays a primary role in the removal of aged RBCs. In order to perform these journeys RBCs must possess and maintain a significant deformability. The main author of this property is certainly the membrane, that ensures both mechanical stability and deformability. After the first proposed model of the RBC membrane skeleton 36 years ago (Lux et al 1979), containing the core elements of the modern model, many additional proteins have been discovered during the intervening decades, and their structures and interactions have been defined (Mohandas et al 2008; Lux 2016). RBC membrane is composed by a fluid double layer of lipids in which approximately 20 major proteins and at least 850 minor ones are embedded (Andolfo et al 2016). The membrane is attached to an intracellular cytoskeleton by protein-protein and lipid-protein interactions that confer the erythrocyte shape, stability and deformability. The transmembrane proteins have mainly a transporter function. However, several of these also have a structural function, usually performed by an intracytoplasmic domain interacting with cytoskeletal proteins. The lipid bilayer acts as a barrier for the retention of cations and anions within the red cells, while it allows water molecules to pass through freely. Human erythrocytes have high intracellular K+ and low intracellular Na+ contents when compared with the corresponding ion concentrations in the plasma. The maintenance of this cation gradient between the cell and its environment involves a passive outward movement of K+, which is pumped back by the action of an ATP-dependent Na+/K+ pump in exchange for Na+ ions. This protein belongs to a class of transmembrane proteins with a transport function (Figure 1.1).

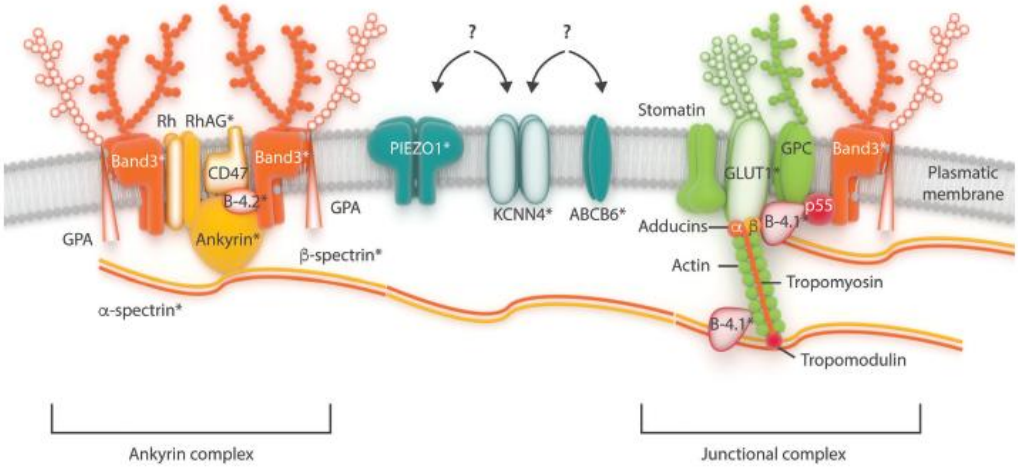

Figure 1.1. Simplified cross-section of the erythrocyte membrane. The red blood cell membrane is composed of integral membrane proteins incorporated into a phospholipid bilayer. The network of cytoskeletal proteins is anchored to the membrane via several transmembrane proteins with a transport function: band 3, anion transporter; GLUT1, glucose and L-dehydroascorbic acid transporter; RhAG, gas transporter, in particular CO2; various cation pumps and transporters including, Na+-K+-ATPase, Ca++-ATPase, Na+-K+-2Cl− and Na+-Cl−, Na+-K+, K+-Cl− co-transporters and Gardos channel. The most recently described proteins PIEZO1, KCNN4 and ABCB6, involved in the modulation of RBC membrane permeability, and their putative interactions are also shown. The relative positions of the proteins to each other within the various complexes are mostly unknown. The shapes of the major proteins are mostly imaginary.
GPA, glycophorin A; Rh, Rhesus polypeptide; B-4.1, protein band 4.1; B-4.2, protein band 4.2; GPC, glycophorin C; RhAG, Rh-associated glycoprotein; RBC: red blood cells. *Proteins that are known to be affected by pathogenic mutations so far.

The third and more important component of the RBC membrane is the cytoskeleton, a protein network that laminates the inner surface of the membrane. Spectrin a and β-chains, proteins 4.1, or 4.1R, and actin are the main components of this skeleton, maintaining the biconcave shape of the RBC. These components are connected to each other in two protein complexes; ankyrin and protein 4.1 complex. The former is composed by band 3 tetramers, Rh, RhAG, CD47, glycophorin A and protein 4.2. Whereas the protein 4.1 complex is composed by band 3 dimers binding adducins a- and β-, glycophorin C, GLUT1 and stomatin (Figure 1.1). The ends of spectrin tetramers converge toward a protein 4.1 complex (junctional complex). Electron microscopy (EM) shows that this latter links the tail of six spectrin tetramers, forming a pseudo-hexagonal arrangement (Liu et al 1987). Spectrin tetramers include anion transporters (band 3 or chloride/bicarbonate exchange). The capability of these transporters to form aggregates could define the half-life of RBCs, causing antibody binding and removal by the spleen. Defects that interrupt this vertical structure (spectrin-actin interaction) underlie the biochemical and molecular basis of hereditary

spherocytosis (HS), whereas defects in horizontal interactions (skeletal attachment to membrane proteins) cause hereditary elliptocytosis (HE).

Membrane protein synthesis is an important part of the differentiation process of erythroid cells in bone marrow and it starts very early. Cell culture studies established that this production is asynchronous (spectrin production starts before the synthesis of other cytoskeletal components) and is quantitatively exuberant (the production of a-spectrin exceeds that of β-spectrin three or four times) (Chen et al 2009). This pattern of production seems to play an important role in the genetics of both HS and HE: as a matter of fact only homozygous or double heterozygous defects of a-spectrin could cause HS; whereas the presence of hypomorphic alleles (such as a-LELY, Low expression Lyon) is completely asymptomatic. However, due to its limiting amount (with respect to a-spectrin), the deficiency of β-spectrin causes HS in the heterozygous state as well. Band 3 and ankyrin synthesis are the latest to occur and they seem to play a critical role in assembly. Protein 4.1 and ankyrin are the last cytoskeletal protein components to continue to be synthesized and assembled. This is at least partly due to the fact that ankyrin and protein 4.1 mRNA persist late into erythropoiesis when the levels of the majority of cytoplasmic RNAs, including those for band 3 and spectrins, have declined precipitously (Andolfo et al 2016).

1.2 Classification, diagnostic criteria and epidemiology of erythrocyte membrane defect-related anemias

From the genetic standpoint, 15 different types of anemias due to RBC membrane defects are currently included in the Online Mendelian Inheritance in Man (OMIM) compendium of human genes and genetic phenotypes (Table 1.1). Of note, the gene mutations identified so far refer only to a restricted number of patients; indeed, the molecular defect is still unknown for several patients. We can divide RBC membrane disorders into two main subgroups: (i) structural defects, and (ii) altered permeability of the RBC membrane. The first subgroup comprises: HS, HE, hereditary pyropoikilocytosis (HPP), and Southeast Asian ovalocytosis (SAO); the second subgroup contains: dehydrated hereditary stomatocytosis (DHS), overhydrated hereditary stomatocytosis (OHS), familial pseudohyperkalemia (FP), and cryohydrocytosis (CHC).

Table 1.1. Classification of HAMDs by OMIM database

Disease symbol	Phenotype	Phenotype MIM number	Gene *location*	Inheritance
HS1	Hereditary spherocytosis type 1	182900	ANK1 *8p11.21*	AD
HS2	Hereditary spherocytosis type 2	616649	SPTB *14q23.3*	AD
HS3	Hereditary spherocytosis type 3	270970	SPTA1 *1q23.1*	AR
HS4	Hereditary spherocytosis type 4	612653	SLC4A1 *17q21.31*	AD
HS5	Hereditary spherocytosis type 5	612690	EPB42 *15q15.2*	AR
HE1	Hereditary elliptocytosis 1	611804	EPB41 *1p35.3*	AD
HE2	Hereditary elliptocytosis 2	130600	SPTA1 *1q23.1*	AD
HE3	Hereditary elliptocytosis 3	-	SPTB *14q23.3*	AD
HPP	Hereditary Pyropoikilocytosis	266140	SPTA1 *1q23.1*	AR
SAO	Ovalocytosis Southeast Asian type	166900	SLC4A1 *17q21.31*	AD
OHS	Overhydrated hereditary stomatocytosis	185000	RHAG *6p12.3*	AD
DHS1	Dehydrated hereditary stomatocytosis with or without pseudohyperkalemia and/or perinatal edema	194380	PIEZO1 *16q24*.3	AD
DHS2	Dehydrated hereditary stomatocytosis 2	616689	KCNN4 *19q13*.31	AD
FP	Familial pseudohyperkalemia 2	609153	ABCB6 *2q35-q36*	AD
CHC	Cryohydrocytosis	185020	SLC4A1 *17q21*.31	AD

AD, Autosomal dominant; AR, Autosomal recessive

1.3 Hereditary anemias due to RBC structural defects

1.3.1 Hereditary spherocytosis

HS is the most common non-immune hemolytic anemia with a prevalence of 1:2000-5000 in the Caucasian population (Bogardus et al 2012). This value is probably higher due to under-diagnosed mild/moderate forms. HS refers to a group of heterogeneous inherited anemias showing a broad spectrum of clinical severity, ranging from asymptomatic to severe transfusion-dependent forms, even within the same family. The intra-familial heterogeneity can be ascribed to the co-inheritance of genetic variants involved in erythrocyte defects themselves or in other disorders,

such as enzymopathies, thalassemias and Gilbert syndrome (Jamwal et al 2016). However, HS clinical findings are summarized by hemolytic anemia, jaundice and splenomegaly. Reticulocytosis (6-10% to 35% in severe cases), increased mean corpuscular Hb concentration (MCHC > 34.5g/dL), increased RBC distribution width (RDW >14), and normal or slightly decreased MCV are the main laboratory findings. Anemia in most patients is mild (Hb >11 g/dL) or moderate (Hb 8-11 g/dL), due to poorly compensated hemolysis (Gallagher 2013). Symptomless or mildly anemic patients are often diagnosed after hemolytic or aplastic crises, while in mildly affected women the condition often becomes evident during pregnancy, but transfusions are required only rarely. A small percentage of patients present a severe form (Hb 6-8 g/dL), which needs regular blood transfusions. One of the most common complications of chronic hemolytic anemia is cholelithiasis, which is more frequent in patients who co-inherited Gilbert Syndrome (Lee et al 2014). Of note, the co-inheritance of HS and Gilbert disease can be misdiagnosed as Crigler-Najjar syndrome type II. The third component of the HS triad is splenomegaly, observed in almost all adult patients. The spleen enlargement is mild or moderate, rarely massive: only one patient with spontaneous rupture has been described (Berne et al 1997), while in few patients splenic infarction has been observed (Jones et al 2015; Suzuki et al 2007). Extramedullary erythropoiesis and iron overload can also be observed. Hemosiderosis is more relevant in transfusion-dependent patients or in those who have co-inherited mutations in the causative genes of hereditary hemochromatosis (Perrotta et al 2008). The diagnosis of HS is based on clinical features, positive familial history and the observation of a peripheral blood (PB) smear, in which a variable percentage of spherocytes, related to the degree of anemia, mushroom red cells, poikilocytosis, acanthocytes and ovalostomatocytes can be found (Figure 1.2) (Da Costa et al 2013). The diagnostic guidelines of HS from the British Committee for Standards in Haematology do not recommend any additional tests for patients with classical clinical features and laboratory data (Bolton-Maggs et al 2012). Whenever necessary, indirect tests can also be performed. Among these, the eosin-5′-maleimide (EMA) binding test shows high sensitivity (92-93%) and specificity (nearly 99%), although a positive test can also be obtained in patients affected by related conditions, such as congenital dyserythropoietic anemia type II (CDA II) (King et al 2008). Additional tests, such as the osmotic fragility (OF) test, acidified glycerol lysis test (AGLT) and the pink test, exhibit lower sensitivity compared to the EMA test (68%, 61% and 91%,respectively). Nevertheless, the combination of

the EMA and pink tests or those of the EMA and AGLT tests improves the sensitivity to 99% and 100%, respectively (Bianchi et al 2012). Ektacytometry is a highly sensitive test of membrane deformability (Gallagher 2013).

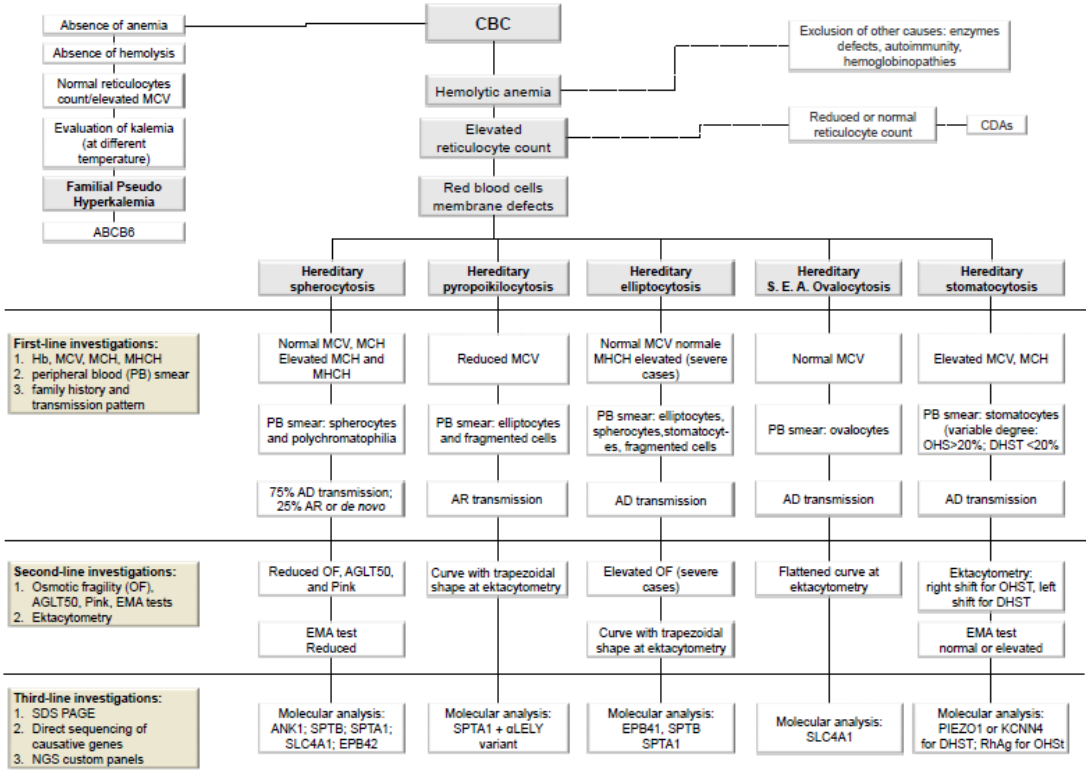

Figure 1.2. Flow diagram for the differential diagnosis of hemolytic anemias due to RBC membrane defects.
The flow diagram shows the main steps for guiding the clinical suspicion toward the diagnosis of different subtypes of hereditary erythrocyte membrane disorders. First-, second-, and third-line investigations are also shown. The cut-off for the EMA binding test is still debated: currently, a test with a reduction of EMA binding > 21%, in comparison with controls, is defined positive, whereas a test with a reduction of EMA binding < 16% is considered negative. Values between 16-21% are not conclusive, although a cut-off of 11% has been proposed. Hb: hemoglobin; MCH: mean corpuscular hemoglobin; MCV: mean cellular volume; MCHC; mean corpuscular hemoglobin concentration; CBC: complete blood count; RBC: red blood cells; OHS: overhydrated hereditary stomatocytosis; DHS: dehydrated hereditary stomatocytosis; AD: autosomal dominant; AR: autosomal recessive; EMA: eosin-5-maleimide; SDS: Sodium dodecyl sulfate; NGS: next generation sequencing; RHAG: rhesus blood group associated glycoprotein. PB: peripheral blood.

In HS the characteristic features of ektacytometry are: decreased DI max, in conjunction with a shift of the Omin point to the right (reduced surface to volume ratio), and a shift of the O' or hyper point to the left (increased dehydration of the red cells) (Figure 1.3) (Da Costa et al 2013).

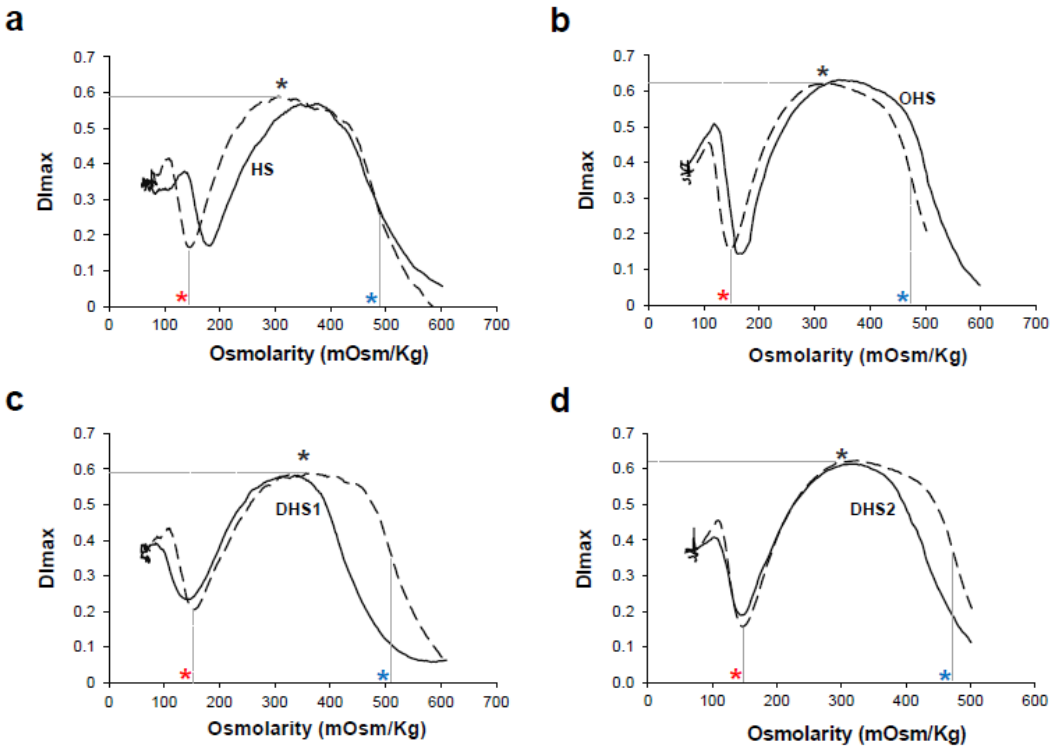

Figure 1.3. Examples of ektacytometric curves of different hereditary erythrocyte membrane disorders.
The ektacytometer is a laser diffraction viscometer that measures RBCs (red blood cells) deformability at constant shear stress as a continuous function of suspending Osmolarity. Three principal features of the osmotic gradient ektacytometry profiles are: the Omin point (red asterisk), which corresponds to the osmolarity at which 50% of the red cells are lysed in the classical osmotic fragility test and represents the surface area to volume ratio; the maximal deformability index (DImax, black asterisk) value, which represents the maximal cellular deformability of the red cell population; and the O' or hyper point (blue asterisk), which corresponds to the osmolarity at DImax/2, which reflects the hydration status of the red cells. Ektacytometric analysis of (A) HS, (B) OHS, (C) DHS1 and (D) DHS2 patients are shown. The dotted line is those relative to the control subjects. HS: hereditary spherocytosis; OHS: overhydrated hereditary stomatocytosis; DHS1: dehydrated hereditary stomatocytosis 1; DHS2: dehydrated hereditary stomatocytosis 2.

As a third-line of investigation, the analysis of major erythrocyte membrane proteins *via* SDS-PAGE still represents invaluable support for the identification of different subsets of HS patients; however, several subjects remain unclassified by this technique. However, the biochemical analyses may be of great use in the interpretation of NGS data in order to assess the pathogenicity of identified genetic variants. In HS, the phenotype variability is linked to different molecular defects. The increased membrane fragility is caused by heterogeneous molecular defects due to deficiency and/or dysfunction in erythrocyte membrane proteins, ankyrin (ANK1), a- and β-spectrin (SPTA and STPB), band 3 (SLC4A1), and protein 4.2 (EPB42) (Andolfo et al 2016). Approximately 75% of HS cases exhibit an autosomal dominant (AD) pattern of inheritance, associated with mutations in

ANK1, *SPTB*, *EPB42* and *SLC4A1* genes. In the remaining 25% of patients autosomal recessive (AR) and *de novo* mutations were observed (Table 1.1).

1.3.2 Hereditary elliptocytosis and pyropoikilocytosis

HE is characterized by the presence of elliptical-shaped erythrocytes (elliptocytes) on the PB smear associated to variable clinical manifestations. The worldwide incidence of HE is 1:2000-4000 individuals, but it results higher in some African regions (1:100). The majority of patients present no anemia or hemolysis, and diagnosis is made incidentally, after worsening of anemia due to infections or after diagnosis in symptomatic relatives. Severe anemia was observed only in rare cases. A good indicator for the severity of the disease is the percentage of spectrin dimers. A subtype of HE is HPP, a rare severe hemolytic anemia characterized by poikilocytosis and fragmented erythrocytes, resulting in low MCV (50-60 fL) and microspherocytes. 16 HPP patients show marked splenomegaly, and splenectomy is therefore usually recommended. There is a strong association between HE and HPP. The main defect in HE erythrocytes is mechanical weakness or fragility of the erythrocyte membrane skeleton due to defective horizontal connections of cytoskeletal proteins, such as spectrin dimer-dimer interactions and spectrin-actin-protein 4.1 at the junctional complex. For the main part, HE is inherited as AD disease, with rare cases of *de novo* mutations, whereas HPP patients exhibit an AR inheritance. HE can be due to mutations in *EPB41*, *SPTA1* and *SPTB* genes that lead to serious damage in the association of spectrin dimers/tetramers (Iolascon et al 2013). Also, HE shows high inter- and intrafamilial phenotypic variability, due to the modifier alleles. One example is the a-LELY in the *SPTA1* gene, a hypomorphic haplotype composed of two variants, the missense Leu1857Val and the splicing variant in intron 45. This hypomorphic haplotype alone causes minimum damage in both heterozygous and homozygous states since the spectrin a chains are produced in excess (3- to 4- fold compared to β-chains); otherwise, when it is associated with a HE mutation in *SPTA1*, the resulting phenotype is severe, i.e. HPP (Table 1.1) (Iolascon et al 2013).

1.3.3 Southeast Asian ovalocytosis

SAO is a very common condition in the aboriginal peoples from Papua New Guinea, Indonesia, Malaysia, the Philippines and southern Thailand, in areas where malaria is endemic, with prevalence varying between 5% and 25%. Indeed, this condition offers protection against all forms of malaria (Iolascon et al 2013).

Despite the reduced *in vitro* deformability of SAO erythrocytes, patients are asymptomatic and the diagnosis is made accidentally as a result of a PB smear examination, showing the characteristic rounded elliptocytes (ovalocytes). However, in newborns it may manifest as hemolytic anemia and require phototherapy. SAO is an AD condition caused by the deletion of 27 nucleotides in the *SLC4A1* gene, leading to the loss of the amino acids 400-408 of protein band 3.2 The deletion is in linkage disequilibrium with the Memphis polymorphism (p.Lys56Glu) in *SLC4A1* (Table 1.1). SAO erythrocytes show a slight loss of monovalent cations when exposed to low temperatures, with a reduction of anions flux. Thus, the condition may be classified as a genetic disease affecting the permeability of the RBC membrane. Despite the frequency of heterozygotes, only one case homozygous for the 27 nucleotide deletion has been described so far. This patient showed severe phenotype with intrauterine transfusions, transfusion dependent anemia and distal renal tubular acidosis due to the loss of band 3, which is also expressed in the kidneys (Picard et al 2014).

1.3.4 Other conditions

Erythrocyte abnormalities can also be observed in other hereditary and acquired conditions. For example, the autoimmune hemolytic anemias are characterized by shortened RBC survival due to the presence of auto-antibodies directed toward red cells, with a positive Coombs test. RBCs are typically coated with auto-antibodies and trapped by macrophages in the cords of the spleen. The interaction of trapped RBCs with splenic macrophages may result in phagocytosis of the entire cell or partial phagocytosis with the formation of spherocytes, present in the blood film (Packman et al 2015). Micro- and macrospherocytes, associated with increased osmotic fragility, were also seen in patients affected by chronic hepatitis C virus treated with protease inhibitors (telaprevir and boceprevir). In these patients oxidative stress, induced by drugs, damages membrane-cytoskeletal stability, reducing a- and β-spectrins (Lupo et al 2016). Alterations in the RBCs membrane are also present in neuroacanthocytosis, a heterogeneous group of diseases that include chorea-acanthocytosis, McLeod and Huntington's disease-like syndromes. These conditions are characterized by alterations of post-translational modifications, mostly phosphorylation, of erythrocyte membrane proteins and significant neurological symptoms (De Franceschi et al 2014).

1.4 Anemias due to altered permeability of RBC membrane

1.4.1 Dehydrated hereditary stomatocytosis or xerocytosis

HST includes both DHS and OHS, which show alteration of the RBC membrane permeability to monovalent cations Na+ and K+, with a consequent alteration of the intracellular cationic content and alterations of cell volume (Delaunay 2007). DHS is the most highly represented among HST, with an incidence of approximately 1:50000 births. It is 10-20 times less frequent than HS, with which it may be, however, confused. Of note, based on our experience, the incidence of this anemia could be underestimated because it is often undiagnosed. The phenotype ranges from asymptomatic to severe forms, with massive hemolysis. Generally, DHS patients show hemolytic well-compensated anemia, with a high reticulocyte count, a tendency to macrocytosis and mild jaundice. The main characteristic of RBCs is cell dehydration caused by the loss of the cation content, with a subsequent increase of MCHC (>36 g/dL). At blood smear the stomatocytes, erythrocytes with a characteristic central mouth-shaped spot, are quite rare, which often makes diagnosis difficult. In addition, it may be difficult when the clinical picture is associated with pseudohyperkalemia and/or perinatal edema, in the so-called pleiotropic syndrome form (Grootenboer et al 2008; Delaunay 2004). For these reasons, the condition may be overlooked for years or decades before reaching a conclusive diagnosis. Osmotic gradient ektacytometry is a useful tool to diagnose this condition; it shows a leftward shift of the minimum in the deformability index (Omin) at low osmolarities, as well as a decrease in DImax (Figure 1.3). DHS patients also exhibit a tendency toward having iron overload, regardless of the transfusion regimen or splenectomy (Syfuss et al 2006). The study of the iron metabolism in this condition is an open and interesting field of investigation, enabling the discovery of new drugs to treat the iron overload. DHS is inherited as an AD trait. The candidate gene locus was first localized at 16q23-24 (Carella et al 1998; Grootenboer et al 2000). Several years later, *PIEZO1* was identified as the causative gene of both isolated and syndromic forms of DHS1 by exome sequencing (Table 1.1) (Zarychanski et al 2012; Andolfo et al 2013). *PIEZO1* encodes a mechanoreceptor, an ion channel activated by pressure. This protein has been identified in the RBC membrane, and in mice it has been shown to form a tetramer of about 1.2 million daltons; it is therefore the largest ion channel identified to date, and moreover it regulates mechanotransductive release of ATP from human RBCs (Coste et al 2010; Ge et al 2015; Cinar et al 2015). The identified mutations are missense and mainly located in the highly conserved C-terminus of

the protein, recently described to form the pore of the channel (Coste et al 2015). Several electrophysiology studies demonstrated that the mutations cause a gain-of-function phenotype with delayed inactivation of the channel (Andolfo et al 2013; Bae et al 2013) suggesting increased cation permeability leads to DHS erythrocyte dehydration (Figure 1.4).

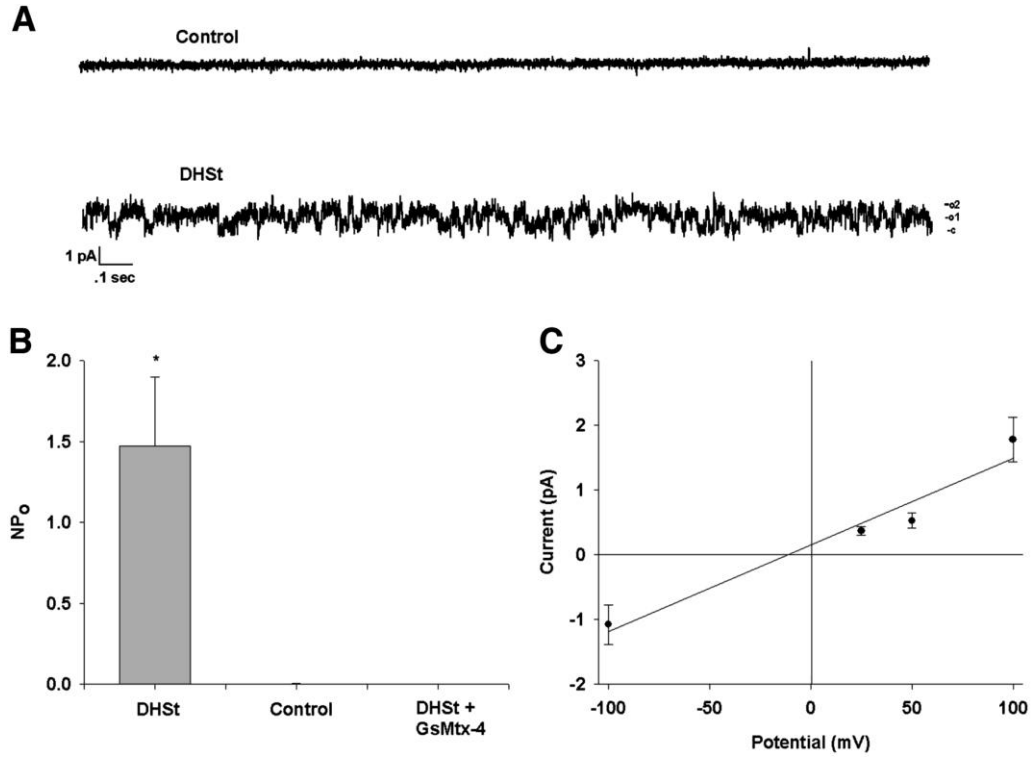

Figure 1.4. Cation channel activity in on-cell patch recordings of a DHSt red cells.
(A) Representative graphs of channel activity in on-cell patches from an unrelated normal cell (above) and a DHSt red cell from patient SF. (B) NPo of channel activity in DHSt red cells from patient SF (n 5 4), from an unrelated volunteer (Control, n 5 3) and from patient SF in the presence of pipet GsMTx-4 (2.5 mM; n 5 3); *P , .05. (C) I-V curve of a representative on-cell patch record from a DHSt red cell of patient SF.

Recently, a novel gene, *KCNN4*, has been identified as causative of a second form of DHS, named DHS2, in six different families (Table 1.1) (Rapetti-Mauss et al., 2015; Andolfo et al., 2015; Glogowska et al., 2015). The *KCNN4* gene encodes the Gardos channel, a widely expressed Ca2+-dependent K+ channel of intermediate conductance that mediates the major K+ conductance of erythrocytes (Andolfo et al 2015; Andolfo et al 2016). Mutated *KCNN4* channels showed a higher current compared to WT resulting from changes in the open probability, in the trafficking, and in the unitary conductance of the channel. This is suggestive of the pathogenic mechanism associated with several mutations affecting PIEZO1. In addition, this observation could suggest that PIEZO1 and the Gardos channel might act in the

same stretch-induced cation pathway involved in cell volume homeostasis. Unlike DHS1, patients affected by DHS2 show a normal pattern of ektacytometry analysis (Figure 1.3), whereas they exhibit iron overload similar to that in DHS1 patients (Rapetti-Mauss et al 2015; Andolfo et al 2015; Glogowska et al 2015).

HST can also be associated with band 3 mutations, characterized by the conversion of band 3 from an anion exchanger to a cation transporter (Iolascon et al 2009).

1.4.2 PIEZO1

PIEZO1 is a cation selective channel activated by mechanical force (Coste et al 2012; Kim et al 2012). It conducts all monovalent cations (Na^+ , K^+ , Li^+ , Cs^+) and also divalent cations, such as Ba^{2+}, Ca^{2+}, Mg^{2+} and Mn^{2+} (Gnanasambandam et al 2015). Its spatial organization has recently been solved and it appears to function as a trimer whose shape looks like a three-blade propeller (Ge et al 2015). Each subunit is structurally divided in 3 parts across the plasma membrane. The first consists of a large extracellular domain composed of the N terminal part of the protein (blade). The second region consists of the C-terminal extracellular domain (CED), a membrane spanning domain with 14 a-helices (the CED is located between helix 13 and helix 14 which is the inner helix facing the transport site); and third, an intracellular domain containing the C terminus (Figure 1.5). In addition to its role in RBC, PIEZO1 plays an important role in the vascular and renal systems (Bae et al 2013b). In 2012 and 2013, 3 different groups described mutations in PIEZO1 as the cause of HX in several unrelated families (Zarychanski et al 2012; Andolfo et al 2013). The substitutions in the mutated form of this protein consist of missense or truncating modifications that cluster in two hot spots located in the highly conserved C terminus pore module of the channel (Bagriantsev et al 2014; Ge et al 2015). For several mutations, the mutated channel has been demonstrated to exhibit greater activity and a slower rate of inactivation (Bae et al 2013b). The longer open state of the channel should drive an excess of K^+ efflux and hence excess water loss. Beside its role in HX, defects in PIEZO1 have also been shown to result in congenital lymphatic dysplasia with the description of loss of function mutations (Fotiou et al 2015). This finding may be related to the fact that foetal oedema without anaemia has been reported several times in patients with HX (Andolfo et al 2013), and to the role of PIEZO1 in the alignment of vascular endothelium and proper blood vessel formation (Ranade et al 2014).

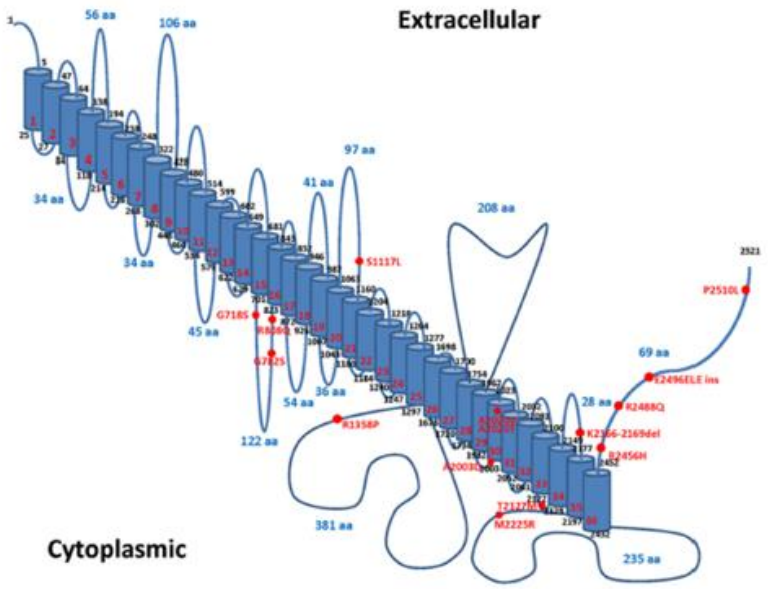

Figure 1.5. Models of human PIEZO1.
Predicted membrane topology models of PIEZO1 (UniProt accession number Q92508) were created using Swiss-Prot prediction tools. The locations of PIEZO1 mutations identified in DHS are indicated.

1.4.3 KCNN4

The Gardos channel The Gardos channel (KCNN4, KCa31, SK4, IK1) is a Ca2+ activated K+ channel of intermediate conductance (Andolfo et al 2016). This channel has been extensively studied in red cells, where it has been shown to decrease cell volume, but also in other cells, such as activated T- and B-cells, macrophages, microglia, vascular endothelium and epithelia, where it is involved in many physiological and pathological mechanisms. Consequently, it is considered as a potential target for therapeutic approaches in various diseases like sickle cell anaemia, asthma, atherosclerosis, kidney fibrosis and autoimmunity (Christophersen et al 2015). The Gardos channel is comprised of 4 identical subunits, each of which is encoded by a single gene, KCNN4, and consists of 6 transmembrane domains and a pore region between transmembrane domain 5 and 6 (Figure 1.6) (Maher et al 2003). In steady state conditions, the Gardos channel is inactive. Its function is not fully elucidated in mature normal erythrocytes; however it is thought to be one of the major players in the RBC volume changes (Thomas et al 2011). Under stimulation, such as external stress, intracellular Ca2+ increases and then interacts with Calmodulin molecules that are bound tightly on each of the four channel subunits of the Gardos channel. Interaction between Calmodulin and Ca2+ results in the opening of the channel and rapid K+ and water efflux leading to

erythrocyte dehydration and shrinkage, a mechanism referred to as the Gardos effect (Maher & Kuchel 2003).

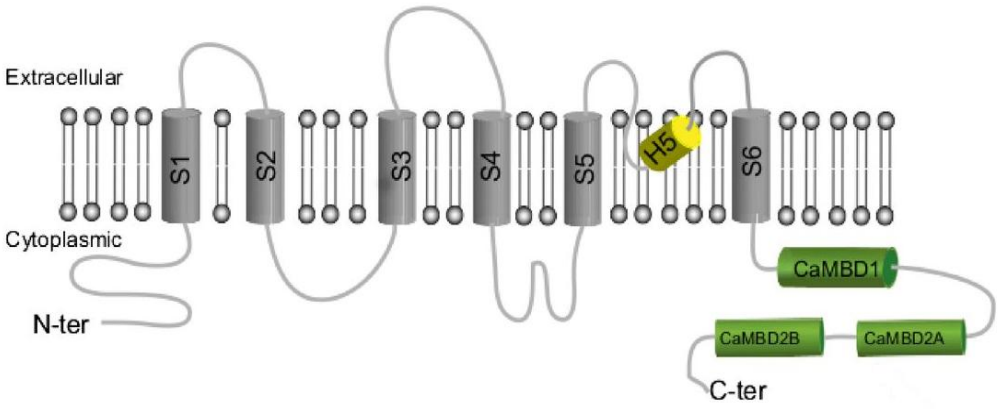

Figure 1.6. Structure of the KCNN4 channel.
Structure of the KCNN4 channel consisting of six transmembrane domains, a pore region (P) between S5 and S6, and calmodulin interacting with the channel's intracellular COOH terminus.

In HX, the R352H mutated Gardos channel is more sensitive to Ca2+ activation, permits an increased efflux of K+ and remains open and active during a prolonged period when compared to the normal channel, leading to excessive RBC dehydration (Rapetti-Mauss et al 2015). A total of 7 independent families have currently been described with HX and mutations in the Gardos channel (Andolfo et al 2015; Glogowska et al 2015; Rapetti-Mauss et al 2015). Recurrent mutations in only 2 different sites account for all cases, the first one being located in the Calmodulin binding region of the channel (R352H) and the other one in the pore-forming region (V282M/E). In one case, channel mutation occurred de novo, strongly suggesting, together with the recurrence, that the residue is, in itself, a hot spot for mutation. Pathophysiological mechanism for HX. Hyper-activation of either PIEZO1 or the Gardos channel leads to similar clinical phenotypes, strongly suggesting that both channels act together to shrink RBC volume under mechanical stress. It is likely that hyperactivity of the Gardos channel is responsible for K+ and water efflux, either because of an activating mutation in Gardos channel or because of mutations in PIEZO1 that would increase intracellular Ca2+ level and subsequently activate Gardos channel. However, PIEZO1 is more selective to K+ than it is to Ca2+ and mutations that prolong the conductive state of the channel (Albuisson et al 2013) are expected to increase the K+ leak through PIEZO1, independent of an eventual activation of the Gardos channel due to increased Ca2+ permeability. Further research on ion selectivity of

mutated PIEZO1 is necessary to fully understand its involvement in red cell dehydration. Although both the PIEZO1 and Gardos channels are expressed in other tissues, dysfunction of these proteins leads to defects only in circulating cells such as RBC. This suggests that compensatory mechanisms might take place specifically in the other tissues where these proteins are expressed.

1.4.4 Overhydrated hereditary stomatocytosis

OHS is a very rare subtype among HST, with 20 cases reported overall worldwide. Contrary to DHS, RBCs are hydrated due to an increase, from 20 to 40 times, in the loss of cations (Andolfo et al 2016) OHS is associated with more severe phenotypes compared to DHS. In addition to reticulocytosis, it is characterized by a sharp increase in MCV (>110 fL) and decreased MCHC (24-30 g/dL). The number of stomatocytes is usually much higher than that observed in DHS. The causative gene of this condition is *RHAG*, encoding the Rh-associated glycoprotein (RhAG) which acts as an ammonia channel (Table 1.1) (Andolfo et al 2016). Stomatin has been found at low or absent levels in OHS patients, but no mutations have been found in the encoding gene so far. Moreover, a complex syndrome named stomatin-deficient cryohydrocytosis has been described. It is characterized by mental retardation, seizures, cataracts and massive hepatomegaly. Recently, this syndrome was associated with mutations in *SLC2A1* that cause both loss of glucose transport and a cation leak (Andolfo et al 2016).

1.4.5 Familial pseudohyperkalemia and cryohydrocytosis

FP and CHC are additional forms of stomatocytosis. FP is not associated with hemolytic anemia and stomatocytes are rarely observable on PB smear. Conversely, CHC patients show hemolytic anemia of variable degrees (Stewart et al 1979). RBCs from FP patients exhibit a loss of K+ at low temperatures (<37°C, mostly 8-10°C), but not at 37°C. In CHC the main feature is the temperature dependence of the loss of cations: instead of being around 8-10°C, the minimum is approximately 23°C. The gene responsible for FP was mapped at 2q35-q36,55 (Carella et al 2004) and later identified in the *ABCB6* gene (Andolfo et al 2013), encoding the homonymous protein, ABCB6. It belongs to the family of ABC transporters with the binding cassette for ATP, one of the most abundant families of integral membrane proteins. ABCB6 was previously identified as a porphyrin transporter, thus we now find that it is currently highly debated because several other studies identified its expression in the plasma membrane of RBCs and in the

endo-lysomal compartment, excluding the mitochondrial uptake of porphyrins (Andolfo et al 2016) Moreover, in erythrocyte membranes it bears the Langereis (Lan) blood group antigen system (Helias et al 2012; Kiss et al 2012). ABCB6 expression increases during erythroid differentiation of CD34+ cells (Andolfo et al 2012).

The ABCB6 missense mutations in FP does not alter mRNA or protein levels, or subcellular localization in mature erythrocytes or erythroid precursor cells, but are predicted to have a pathogenic consequence on protein function. CHC is due to mutations in the *SLC4A1* gene; these are gain-of-function mutations, since they are able to transform the band 3 anion exchanger to a cation transporter (Table 1.1).

1.4.6 ABCB6

ABCB6 belongs to the family of ATP-binding cassette (ABC) transporters, one of the most abundant families of integral membrane proteins (Zutz et al 2009).The ABC transporters couple ATP binding and hydrolysis to the transport of endogenous and xenobiotic substrates across cellular membranes. ABCB6 is a member of the B (MDR/TAP) subfamily of ABC transporters best known as drug-resistance genes, and it can form homodimers (Krishnamurthy et al 2006). Indeed, increased ABCB6 expression correlates with increased drug resistance in multiple cell lines (Szakacs et al 2004). A specific ABCB6 function was first described in *Saccharomyces cerevisiae* mutants lacking mitochondrial ABC transporter Atm1p (Mitsuhashi et al 2000). Complementation of Atm1p-deficient yeast with human ABCB6 rescued the phenotypic alterations, leading to the proposal that ABCB6 is the human ortholog of Atm1p (Mitsuhashi et al 2000). In 2006, ABCB6 was shown to catalyze mitochondrial uptake of coproporphyrin III, as an important regulator of cellular porphyrin biosynthesis (Krishnamurthy et al 2006). However, Tsuchida questioned the mitochondrial localization of ABCB6, providing evidence for its localization in endoplasmic reticulum and Golgi membranes, rather than in mitochondria (Tsuchida et al 2008). The observation of extra-mitochondrial localization has been extended by the study of dominantly inherited ABCB6 mutations in patients with ocular coloboma and dyschromatosis universalis hereditaria (Liu et al 2014; Wang et al 2012). Gene expression profiling studies of zebrafish blood formation mutants revealed ABCB6 among genes of the erythroid cluster (Weber et al 2015). ABCB6 was recently shown to carry the Lan (Langereis) blood group antigen system of the RBC plasma

membrane (Helias et al 2012). The asymptomatic Lan (-/-) carriers display a variety of recessive null mutations, all with red cells of normal phenotype (Helias et al 2012). Lan blood group mismatch can cause hemolytic transfusion reactions and hemolytic disease of the newborn. Kiss recently confirmed ABCB6 as a glycoprotein present in the membrane of mature erythrocytes and in exosomes released from reticulocytes during the final steps of erythroid maturation (Kiss et al 2012). Knockdown studies demonstrated that ABCB6 function is not required for *de novo* heme biosynthesis in differentiating K562 cells, excluding this ABC transporter as an essential regulator of porphyrin synthesis.

In the study of identification of ABCB6 as causative of FP, we confirm that ABCB6 is upregulated during erythroid differentiation and is localized at the plasma membrane in mature RBCs and in CD34+ during the erythroid differentiation (Andolfo et al 2013). Abcb6-/- mice exhibit a grossly normal phenotype, but lack ATP-dependent mitochondrial uptake of coproporphyrin III. ABCB6 deficiency upregulates heme and iron pathways that are necessary for normal development. However, in conditions of extreme demand for porphyrins (such as during phenylhydrazine stress), these adaptations appear inadequate, suggesting the importance of ABCB6 for optimal survival under these stress conditions (Ulrich et al 2012).

1.5 Animal models

Several animal models have been developed for the study of RBC defects (Table 1.2). Concerning the mouse models, although the main stream of human hemolytic anemias caused by RBC membrane defects are inherited as AD, in mice these conditions are usually inherited as AR (Table 1.2). Recently, within hereditary stomatocytosis, mouse models of PIEZO1 were developed. Mice deficient in Piezo1 die *in utero* at mid-gestation due to defective vasculogenesis (Cahalan et al 2015). Thus, another model of Piezo1 was developed by specific deletion in the hematopoietic system (Vav1-P1cKO mice). Hematological analysis of blood from Vav1-P1cKO mice revealed elevated MCV, MCH and reduced MCHC. RBCs exhibited increased osmotic fragility, demonstrating that Piezo1-deficient RBCs were overhydrated. At the moment a knock-in mouse model carrying missense mutations found in DHS1 patients doesn't exist; its creation will further elucidate the role of PIEZO1 in the hydration pathways of RBCs. Beyond mouse models, which in several cases don't recapitulate the main characteristics of human hematological

disease, a powerful model for the study of erythropoiesis is the zebrafish, *Danio rerio*, because of its small size, its ability to generate a large number of embryos, and its transparency that facilitates the visualization of erythroid cell migration (Kulkeaw et al 2012). Notably, the high conservation of hematopoietic genes among vertebrates and the ability to successfully transplant hematopoietic cells have enabled the establishment of models of human anemic diseases in zebrafish (Table 1.2). Recently, zebrafish models have also been created for PIEZO1. Morpholino-knockdown of Piezo1 expression in the *Danio rerio* was reported to result in severe anemia (Faucherre et al 2014). However, the phenotype observed in the morpholino-knockdown model was not present in an independent zebrafish model carrying a predicted truncated form of PIEZO1 (Table 1.2) (Shmukler et al 2015). The debate on the phenotype observed in the two different models is still open (Shmukler et al 2016; Faucherre et al 2016). It is notable that patients with homozygous loss-of-function mutations in human *PIEZO1* show lymphatic dysplasia and an asymptomatic, fully compensated, very mild hemolytic state of incomplete penetrance (Fotiou et al 2015). In conclusion, both mouse and zebrafish models appear not to better recapitulate the human pathogenesis, but they are useful to study the function of newly identified proteins such as PIEZO1.

Table 1.2. Animal models for the study of RBC membrane defects

Organism	Mutant	Altered gene	Type of alteration	Phenotype	PUBMED ID[§]
Mus musculus	ja/ja	SPTB	Deficiency of β-spectrin	Severe hemolytic anemia, reticulocytosis	7937844
	sph/sph	SPTA	Deficiency of α-spectrin		11920196
	Nan	KLF1	Missense E339D	Neonatal anemia; in adult mice, hemolytic anemia with decreased RBCs, hematocrit, Hb, and elevated zinc protoporphyrin levels	20691777
	ENU-generated	ANK1	Nonsense E924X	Heterozygous mice: low MCV, elevated RBC counts, reticulocytosis, reduced EMA intensity, and increased osmotic fragility	21193012
	wan	Slc4a1	Premature stop codon	Homozygous mice: severe anemia with marked anisocytosis and spherocytosis at the PB smear	15070709
	sph^{Dem}/sph^{Dem}	SPTA	In frame deletion of 46 amino acids that alters spectrin dimer/tetramer stability	Increased MCV, decreased MCHC, marked reticulocytosis (50%). PB smears: elliptocytes, spherocytes and occasional poikilocytes, as seen in human severe HE	11154235
	Vav1-P1cKO	PIEZO1	Gene deletion in the hematopoietic system	Elevated MCV, MCH and reduced MCHC. RBCs exhibit increased osmotic fragility	26001274
Danio rerio	merlot	EPB41	Mutation	Spiculated RBC membranes; hemolytic anemia, cardiomegaly, splenomegaly	12183387
	Morpholino	PIEZO1	knockdown of gene expression	Severe anemia with swollen, fragile and spherocytic RBCs	23872304
	ZFN knockout	PIEZO1	Frameshift in the exon 8	No anemia or dysmorphic erythrocyte morphology	26294733

2. AIMs of the study

This PhD program is focused on the study of molecular genetics and pathogenetic mechanism of two inherited haemolytic anemias: Isolated Familial Pseudohyperkalemia (FP) and Dehydrated hereditary stomatocytosis (DHS). Both conditions are included in the group of hereditary membrane defects of RBCs characterized by alterations of the ionic transport across the cellular membrane. Three years ago our group identified disease causing genes of both the conditions: *ABCB6* for FP and *PIEZO1* for DHS (Andolfo et al 2012; Andolfo et al 2013).

The aims of this program are:

AIM 1: Functional characterization of ABCB6 mutants to understand the pathogenetic mechanism of FP and its implication in blood transfusion

AIM 2: Identification of other causative gene/s of DHS by whole exome sequencing in those cases negative for mutations in *PIEZO1*

AIM 3: Functional characterization of *PIEZO1* and *KCNN4* mutations to understand the molecular pathogenesis of DHS.

3. Materials and Methods

3.1 Collection of all patients

Up to now we enrolled the largest cohort of patients with DHS and FP: 97 affected subjects from 41 unrelated families of Italian and foreign countries. This is associated with clinical record data and DNA/RNA/plasma membrane protein bank. For all patients we have recruited hematological and iron metabolism parameters.

3.2 FP patients

Three new patients with FP from three independent pedigrees were enrolled in this study (see Table 4.1 in the “Results” section), and blood samples were obtained from affected patients. Whenever possible, relatives were also investigated. Diagnosis was based on history, clinical findings, laboratory routine data, peripheral blood smear, and genetic testing. Information about every clinical characteristic was not available for all cases. A cohort of 327 blood donors from the blood transfusion center of the Cardarelli Hospital in Naples was enrolled to undergo genetic screening for the ABCB6 mutations found in this study.

Collection of patient data and samples was obtained by the clinicians responsible for patient care with informed consent according to the Declaration of Helsinki and with approval by local university ethical committees.

3.2.1 Whole exome sequencing (WES) of FP Irish family

Blood was obtained for genetic analysis from affected and unaffected family members of the Irish family and from healthy controls, with signed informed consent according to the Declaration of Helsinki. Blood collection was according to protocols approved by local university ethics committees. Genomic DNA was prepared from peripheral blood with the Wizard Genomic DNA purification kit (Promega, Milano, Italy). Five µg of DNA from two affected and two unaffected members of DHS Irish family was diluted in 700 µl of Nebulization buffer (Illumina, San Diego, CA) and sheared by nebulizers (Invitrogen, Carlsbad, CA) into fragments of 200–400 bp in length (Bioanalyzer 2100, Agilent, Santa Clara, CA). Sheared samples purified by QIAquick spin columns (Qiagen, Hilden, Germany) were processed for library preparation (Illumina protocol), omitting size-selection of adapter-ligated fragments prior to capture. After several cycles of PCR amplification, 500 ng of DNA from the resulting libraries was hybridized to the bait set from the SureSelect Human All Exon Kit (Agilent, Santa Clara, CA, USA) at

65°C for 24 h. Hybrid capture with streptavidin-coated Dynal magnetic beads (Invitrogen, Carlsbad, CA) was performed as manufacturer's protocol. Captured samples were further purified through Agencourt AMPure XP beads and subjected to PCR amplification. All samples at each step of library preparation were quantified by Bioanalyzer 2100 (Agilent). Individual sample libraries were NaOH-denatured and loaded onto one lane of an Illumina Flowcell v4. DNA clusters were generated through a one-step workflow on the Cluster Station using TruSeq PE Cluster Kit v5 (Illumina, San Diego, CA). A PhiX control library added to each sample at 1% volume served as internal control. Sequencing was performed on the Illumina Genome Analyzer IIx platform as paired-end 100-bp reads according to the manufacturer's protocol. An exome capture was considered successful if >80% of the target regions were covered with a high quality genotype. Reads were aligned to the most recent version of human genome (GRCh37/hg19) using the BWA software package v0.5.

3.2.2 Sanger sequencing analysis of ABCB6 gene

The search for mutations was performed by direct sequencing, using 75 ng genomic DNA. All exons and flanking splice junctions of the *ABCB6* gene were amplified by PCR in a 25 µl volume with Master Mix 2X (Promega). Oligonucleotide primers were designed by the program Primer3 v.0.4.0. Integrity of PCR products was checked by agarose gel electrophoresis. Direct sequencing was performed using the BigDye® Terminator Cycle Sequencing Kit (Applied Biosystems, Branchberg, NJ, USA) and a 3730 DNA Analyzer (Applied Biosystems). Missense substitution mutations in ABCB6 (Q9NP58) were evaluated by Poly-Phen-2 (http://genetics.bwh.harvard.edu/pph2/index.shtml) and SIFT (http://sift.jcvi.org/) online tools.

3.2.3 ABCB6 screening in donor blood subjects

Mutation screening for *ABCB6* variants R276W, V454A, and R723Q in a population of 327 blood donors was performed by amplification-refractory mutation system (ARMS) analysis, using allele specific tetra-primer ARMS-PCR primers designed by PRIMER1 (http://primer1.soton.ac.uk/primer1.html).

3.2.4 Bioinformatic modeling of ABCB6 protein structure

To assess the potential effects of the identified mutations on protein structure, we generated 3D structural models of dimeric human WT ABCB6 residues 231–827

and the corresponding regions of FP mutant ABCB6 polypeptides V454A, R276W, and R723Q. Sequences were aligned in ClustalW2. MODELLER v9.913 was used for homology modeling in both inward- and outward-facing 6 conformations. The best five structural models with lowest objective function values (as implemented in MODELLER) were subjected to energy minimization in GROMACSv4.5.414.

Structural models were converged using steepest descent energy minimization with 1,000 steps of step size 0.01 nm. Stereochemical quality of each energy-minimized structure was assessed by PROCHECK15. The average of three models of highest stereochemical quality was chosen for ABCB6 structural models. 3D structural models were visualized and aligned using MolMol16 and PyMOL 1.5.0.4 (Schrödinger, LLC).

3.2.5 Molecular cloning of ABCB6 and site-directed mutagenesis

To detect and determine the inheritance pattern of the two mutations in patient Cardiff 2, the DNA fragment encompassing the two mutations R276W and R723Q, of ABCB6 was PCR amplified and cloned into PCR Cloning Vector pSC-A-amp/kan (StrataClone PCR Cloning Kit, Agilent). Point mutations c.1123 C>T, p.R375Q; c.1361T>C; p.V454A; c.826G>T; p. R276W; c.2168G>A; p.R723Q; c.1124 G>A; p.R375W were introduced into pcDNA3.1-ABCB6 with the QuikChange kit (Stratagene, La Jolla, CA). The integrity of the complete ABCB6 coding region was confirmed by sequencing after mutagenesis. Primers sequences are available upon request.

3.2.6 Cell culture and transfection assay for ABCB6

Human HEK-293 cells were maintained in DMEM medium (Sigma) supplemented with 10% fetal bovine serum (FBS), 100 U/mL penicillin, and 100 mg/mL streptomycin (all from Life Technologies), in a humidified 5% CO_2 atmosphere at 37°C. pcDNA3.1-ABCB6-WT and pcDNA3.1-ABCB6 mutant constructs (5µg) were transfected into HEK-293 cells using X-tremeGENE HP DNA Transfection Reagent (Roche, Indianapolis, IN, USA). To phenocopy the heterozygous genotypes, cells were transfected with 2.5µg of WT pcDNA3.1-ABCB6-WT plus 2.5µg of pcDNA3.1-ABCB6 mutants R375Q, p.R276W or R375W.

For the compound heterozygous genotypes, cells were transfected with 2.5µg pcDNA3.1-ABCB6-R276W plus 2.5µg pcDNA3.1-ABCB6-R723Q. For the homozygous genotype, cells were transfected with 5µg pcDNA3.1-ABCB6-V454A. After 72 hrs, cells were harvested for analysis.

3.2.7 Immunofluorescence analysis of ABCB6

HEK-293 cells ($2x10^6$) on coverslips were transfected with ABCB6 cDNAs as previously described (Andolfo, 2012). After 72 hrs, cells were fixed, and immunostained with anti-FLAG (1:200; F3165, Sigma) and anti-WGA (Wheat Germ Agglutinin, Alexa Fluor 555 Conjugate, Life Technologies). Secondary antibodies for FLAG (Alexa Fluor 488 goat anti-mouse; Life Technologies) were incubated at 1:200 dilution in PBS for 30 min at room temperature. Nuclei were stained with 1 µg/ml DAPI in PBS for 15 min at room temperature. The coverslips were mounted in 50% glycerol (v/v) in PBS and imaged by Zeiss LSM 510 Meta confocal microscope equipped with an oil immersion plan Apochromat 63× objective 1.4 NA, Green channel excitation of Alexa488 by the argon laser 488 nm line was detected with the 505-550 nm emission bandpass filter. Red channel excitation of Alexa546 by the Helium/Neon laser 543 nm line was detected with the 560-700 nm emission bandpass filter (using the Meta monochromator). Blue channel excitation of DAPI by the blue diode laser 405 nm line was detected with the 420-480 nm and emission bandpass filter.

3.2.8 Measurements of K+ fluxes in red blood cells of blood donor carrying ABCB6 R276W variant

Blood samples from the donor carrying the *ABCB6* R276W mutation and from two controls obtained from the transfusion center of the Cardarelli Hospital (Naples) were stored four weeks at 4°C in Citrate Phosphate Dextrose Solution (CPD) as anticoagulant, under blood bank conditions. During the four weeks' storage, plasma potassium levels were measured in triplicate by atomic absorption spectroscopy (ANALYST 2000, Perkin-Elmer). The RBCs were gently washed with a buffer containing (in mM) 150 choline chloride, 1mM MgCl2, 10mM Tris MOPS, then lysed for intracellular K measurement by atomic absorption spectroscopy. The free Hb levels were measured to evaluate the degree of hemolysis as for K.

3.2.9 Measurements of ouabain-plus-bumetanide-resistant Rb+ and K+ fluxes in ABCB6 transfected HEK-293 cells

HEK-293 cells at 72 h post-transfection were maintained for 8h under shear stress (rotary shaking at 70 rpm 30°C) in a K+-free medium containing (in mM) 140 NaCl, 5 mM RbCl, 2 CaCl2, 1 MgCl2, 10 HEPES, 10 glucose, with added 10 µM ouabain and 10 µM bumetanide. At the end of the incubation, cell viability was determined by trypan blue staining and medium was removed for extracellular K determination.

Cells were gently washed in buffer containing (in mM) 150 choline chloride, 1mM MgCl2, 10mM Tris MOPS, then lysed for intracellular Rb measurement. Cell Rb content and medium K content were determined in triplicate by atomic absorption spectroscopy (ANALYST 2000, Perkin-Elmer) as previously described (De Franceschi et al 2007).

3.2.10 RNA isolation, cDNA preparation and quantitative qRT-PCR

Total RNA was extracted from cell lines and peripheral blood samples from patients and healthy controls using Trizol reagent (Life Technologies). Synthesis of cDNA from total RNA (2 µg) was performed using Super Script II First Strand kits (Life Technologies). Quantitative RT PCR (qRT-PCR) was by the SYBR-green method using the ABI PRISM 7900HT Sequence Detection system. Relative gene expression was calculated using the 2(-ΔCt) method, where ΔCt indicates the differences in the mean Ct between selected genes and the internal control (GAPDH or β-actin). Sequences of the qRT-PCR primers designed for each gene using Primer Express 2.0 (Life Technologies).

3.2.11 Immunoblotting

Total cell lysates (80 µg protein) electrophoresed on SDS-polyacrylamide gels were electroblotted onto polyvinylidene difluoride membranes (BioRad, Milan, Italy), incubated with the following antibodies: anti-FLAG (1:500; F3165, Sigma), anti-β-actin antibody (1:1000; Sigma, used as loading control), then imaged with HRP-conjugated anti-rabbit Ig (1:5000) (GE Healthcare, UK) and enhanced chemiluminescence substrate (Supersignal West Pico Chemiluminescent Substrate Kit, ThermoScientific, Miami USA). Labeled bands were visualized and densitometric analysis performed with the BioRad Chemidoc using Quantity One software (BioRad).

3.2.12 Statistical analysis

Data are presented as means ± standard error of the mean (s.e.m.). Statistical significance was calculated using the Mann-Whitney test and Student's t test. Correlation analysis was calculated using Spearman's rank correlation coefficient and Pearson's correlation coefficient. $P < 0.05$ was considered as statistically significant.

3.3 DHS patients recruitment for the identification study of new causative gene/s

Fifteen subjects from two independent families, previously screened for PIEZO1 mutations, were enrolled in this study, an Italian family from Naples (family NA) and an American family from Worcester (family WO). The clinical data of the index cases are described in Table 4.5 (see “Results” section) as obtained by the clinicians responsible for patient care, and with the approval of local university ethical committees. All blood samples were obtained with informed consent. The diagnosis of DHS was based on history, clinical findings, routine laboratory data, peripheral blood smear, and genetic testing. DNA was obtained for genetic analysis from affected and unaffected family members, and from healthy blood donors after signed informed consent, according to the Declaration of Helsinki, and as approved by local university ethical committees.

3.3.1 Whole exome sequencing and sequencing analysis of KCNN4 gene

WES analysis was performed as described in paragraph 3.2.1. The search for mutations in *KCNN4* gene was performed by direct sequencing, as already described for *ABCB6* gene in the paragraph 3.2.2. Missense substitution mutations in KCNN4 (O15554) were evaluated by the aforementioned online tools, Poly-Phen-2 and SIFT. Genotyping was also performed by sequencing KCNN4 cDNA prepared by RT-PCR from whole blood (see paragraph 3.3.4) from family WO members III.5, III.6, III.11, IV.5, IV.10, and IV.14.

3.3.2 Isolation and erythroid differentiation of CD34+ hematopoietic progenitor cells

Peripheral blood was collected from four healthy volunteers (with consent according to Declaration of Helsinki) and processed within 24 h. Mononuclear cells were isolated using Ficoll-Hypaque (1.077–0.001 kg/L; Sigma-Aldrich, Milan, Italy). The remaining RBCs were lysed by resuspension of the cell pellets in lysis buffer (155 mM NH4Cl, 10 mM KHCO3, 0.1 mM EDTA). CD341 cells were isolated by positive selection using the miniMACS immunomagnetic isolation system (Miltenyi Biotec, Glodbach, Germany), with >95% yield. These CD34+ cells were cultured at 10^5 cells/mL in a-MEM (GIBCO, Grand Island, NY) supplemented with 30% FBS (GIBCO) and with 2 mM L-glutamine, 1 mM hydrocortisone, 0.1 mM mercaptoethanol, 1% bovine serum albumin (BSA) in deionized water, 10 U/mL Penicillin/Streptomycin (Pen/Strep), 25 µg/mL gentamycin, (Sigma, St. Louis, MO).

To induce erythroid differentiation of CD34+ cells, 10 U/mL recombinant human erythropoietin (rHuepo, Janssen-Cilag, Milan) was added to complete a-MEM medium, and cells were incubated 14 days at 378C in a 5% CO_2 atmosphere. Cell samples were collected on days 0, 7 and 14 for determination of cell number and viability (Trypan Blue exclusion). Erythroid differentiation was assessed by expression of transferrin receptor-1 (CD71) and glycophorin A (CD 235A) as detected by FACS.

3.3.3 K562 cell culture and erythroid differentiation

K562 human myeloid leukemia cells (ATCC, Manassas, VA) were maintained in RPMI medium (Sigma, Aldrich) supplemented with 10% FBS (Sigma, Milan) and Pen/Strep (Sigma, Milan) and grown in humidified 5% CO_2 at 37°C. 50 µM hemin (Sigma, Milan) was added to the culture medium to initiate erythroid differentiation (2-3x10^5/mL). Samples were collected at specific time points: before hemin addition (0D), and at days 4 and 6 after hemin addition. Erythroid differentiation was assessed by FACS detection of transferrin receptor 1 (CD71) and glycophorin A (CD235A).

3.3.4 RNA isolation, cDNA preparation, and quantitative qRT-PCR.

Total RNA was extracted from cell lines and peripheral blood samples from patients and healthy controls using Trizol reagent (Life Technologies). cDNA synthesis from total RNA (2 µg) was performed using Super Script II First Strand kits (Life Technologies). Quantitative RT-PCR (qRT-PCR) was by the SYBR-green method, following standard protocols with an Applied Biosystems ABI PRISM 7900HT Sequence Detection system. Relative gene expression was calculated using the $2^{(-DCt)}$ method, where DCt indicates the differences in the mean Ct between selected genes and the normalization control (GAPDH or b-actin). qRT-PCR primers for each gene were designed using Primer Express software version 2.0 (Life Technologies).

3.3.5 Red blood cell membrane preparation.

Peripheral blood from healthy controls was lysed by three freeze-thaw cycles in 5mM KH2PO4 containing protease inhibitor cocktail (Calbiochem, Merck KGaA, Darmstadt, Germany, set III, animal-free). The membrane fraction was sedimented by lysate centrifugation at 36,000 g for 20 min at 48C. Membrane extracts were loaded on SDS-polyacrylamide gels as described for total cell lysates.

3.3.6 Mouse embryo collection and Immunoblotting

C57BL6/J mouse embryonic tissues were collected at E9.5, E10.5, E12.5, E15.5 as previously described (Andolfo et al 2013). Immunoblotting. Total cell lysates (80 µg protein) were subjected to SDS-PAGE, transferred to polyvinylidene difluoride membranes (BioRad, Milan, Italy), then incubated with the following antibodies: polyclonal rabbit anti-ABCB6 (1:250; SAB1300078, Sigma, Milan, Italy), polyclonal rabbit anti-PIEZO1 (1:500; Proteintech 15939-1-AP), anti-EPB72 (1:200; GeneTex, CA), monoclonal anti-band3 (1:200, Santa Cruz Biotechnology, CA), monoclonal anti-b-actin antibody (1:1000; Sigma, used as loading control), and HRP-conjugated anti-rabbit Ig (1:5000) (GE Healthcare, UK). Blots were incubated in enhanced chemiluminescence substrate (Supersignal West Pico Chemiluminescent Substrate Kit, Thermo- Scientific, Miami, USA). Labeled band visualization and densitometric analysis were by Chemidoc imager and Quantity One software (BioRad).

3.3.7 Statistical analysis

Data are presented as mean ± standard error (SE). Statistical significance was calculated using the Student's t test and one-way ANOVA. $P<0.05$ was considered as statistically significant.

3.4 DHS patients collection for PIEZO1 study

Twelve subjects from two independent families, were enrolled in this study, an English family from Jersey island (family 1) and an Italian family from Bari (family 2). The clinical data of the index cases were obtained by the clinicians responsible for patient care, and with the approval of local university ethical committees. All blood samples were obtained with informed consent. The diagnosis of DHS was based on history, clinical findings, routine laboratory data, peripheral blood smear, and genetic testing. DNA was obtained for genetic analysis from affected and unaffected family members, and from healthy blood donors after signed informed consent, according to the Declaration of Helsinki, and as approved by local university ethical committees.

3.4.1 Direct sequencing of PIEZO1

Genomic DNA preparation and sequencing analysis was performed as described elsewhere (paragraphs 3.2.2 and 3.3.1). In this case our primers were designed to avoid amplification of Piezo2 , Piezo1P1 and Piezo1P2 (Ensembl Gene ID

ENSG00000154864, ENSG00000233686, ENSG00000237121). Missense substitution mutations in PIEZO1 (Q92508) were evaluated by the aforementioned Poly-Phen-2 and SIFT programs.

3.4.2 Cloning, site direct mutagenesis and transfection assay

cDNAs encoding full-length wildtype PIEZO1 were cloned in pLVX-EF1α-IRES-ZsGreen1 vector. The point mutations c.7473_7478dupGGAGCT, p.Glu2492_Leu2493dup and c.5591G>A, p.Arg1864His were introduced into pLVX-EF1α-IRES-ZsGreen1-PIEZO1 by site-directed mutagenesis. The constructs obtained were transfected into HEK-293 cells for 72h as for ABCB6 constructs (see paragraph 3.2.4).

3.4.3 Measurements of ouabain-plus-bumetanide-resistant Rb+ and K+ fluxes in PIEZO1 transfected HEK-293 cells

For the evaluation of ouabain-plus-bumetanide-resistant Rb+ and K+ fluxes in PIEZO1 transfected HEK-293 cells, we performed the same assays described for ABCB6 (see paragraph 3.2.9).

3.4.4 Osmotic gradient ektacytometry

Deformability of the RBCs of the patients and relative control subjects were evaluated by osmotic gradient ektacytometry using the Laser-assisted Optical Rotational Cell Analyzer (LORCA).

4. Results

4.1 Functional characterization of ABCB6 mutations in FP

4.1.1 Case Reports

The Bolivian patient is a 41 year old female from a consanguineous family. Multiple outpatient blood samples indicated elevated plasma K+ (8.3 mmol/L). Renal and adrenal function and EKG were normal, as were hematological indices except for macrocytosis (MCV 95-98 fL; Table 4.1). Past medical history included premature menopause and migraines. Physical examination was unremarkable.

Patient Cardiff-2 is a 35 year old female with a prior tentative diagnosis of hereditary spherocytosis with a positive family history, despite a normal red cell eosin maleimide (EMA) binding test. Outpatient values of plasma [K+] ranged between 8.0 and 8.6 mmolL, in contrast to hospital clinical values between 5.4 and 5.9 mmol/L (Table 4.1). The patient had been under outpatient care for diabetes and other conditions since 1999. Her peripheral blood smear revealed polychromasia, target cells, and a few spherocytes. Past medical history included Irritable Bowel Syndrome, oophorectomy in 2007, splenectomy secondary to trauma in 2008, and diagnosis of depression in 2009. Medications included omeprazole, mebevirine and citalopram. Blood pressure was normal, as was the remainder of the physical exam. Absolute reticulocyte count was 176.0 x109 (4.10 %) with mean reticulocytes volume of 118 fl (reference range 90-110 fl).

The large Irish family was originally described by Stewart and colleagues18 as autosomal dominant dehydrated hereditary stomatocytosis (DHSt) with FP. The propositus developed several thrombotic episodes following splenectomy at age 40 years. An increased passive K+ leak was noted (Table 4.1).

The families Lille, Falkirk and East London were previously described (Andolfo et al 2013). Affected individuals from Family Lille (of Flemish descent) presented with normal hematological indices except for a slightly elevated MCV. Affected from family FP Falkirk (of Pakistani origin) also presented with macrocytosis. Affected from family FP ‘‘East London’’ (of Bangladeshi origin) were anemic and hyperkalemic, but in the absence of reticulocytosis and jaundice were considered non hemolytic.

None of the carriers had colobomatous abnormalities of iris or retina, also associated with missense *ABCB6* mutations. Carriers were not tested for Lan (-/-) status, as this phenotype is caused by nonsense mutations that cause complete absence of ABCB6 polypeptide in circulating red cells.

Table 4.1. Clinical data of FP patients

Family code	Ethnicity	Hb (g/dL)	MCV (fL)	MCH (pg)	K^+ (mmol/L) (< 37°C)
Normal range		*12-18*	*80-95*	*25-31*	*3.5-4.5*
Bolivian	South America	13	95-98	29.3	8.3-8.7
Irish	Ireland	14.8-15.8	95-98	33.7	6.7-7.6
Cardiff-2	United Kingdom	11.9-12.3	116	32.3	8-8.6
Lille #	France	13.7	96	30.7	4-5.5
Falkirk #	Pakistani	11.3-14-7	81-105.5	34.3	7-8.2
East London #	Bangladesh	12-14.2	97	32.6	7-13.7

In bold are the previously unreported families included in this study.
These families was previously described (Andolfo, 2012).

4.1.2 ABCB6 mutational analysis in FP families and blood donor screening

We sequenced the *ABCB6* gene in two patients and one family with FP. In the Bolivian patient we found the homozygous mutation c.1361T>C; p.V454A, while in patient Cardiff-2 we found compound heterozygosity for the two mutations c.826G>T; p.R276W and c.2168G>A; p.R723Q (Table 4.2). Parents of both patients were unavailable for genetic analysis. To analyze the allelic pattern of the two mutations in patient Cardiff-2*,* we cloned the genomic region encompassing both ABCB6 variants (about 6 Kb) into a plasmid vector. DNA sequencing of this cloned region demonstrated that the two mutations are *in trans* in patient Cardiff-2. In the Bolivian patient, the presence of heterozygous SNPs excluded the possibility of a deletion within the region of the gene harboring the mutation.

The Irish family originally diagnosed as DHS plus FP was at first mapped to chr.1619 but subsequent analysis of the *PIEZO1* gene was negative. We therefore subjected the Irish family to WES analysis and identified *ABCB6* variant c.826G>T; p.R276W, with subsequent confirmation by direct sequencing. Probably, there was a misassignment in the Irish pedigree linkage analysis, however, we cannot rule out the presence of intronic mutations that could explain epistasis between PIEZO and ABCB6.

ABCB6 amino acid residues R276, R723 and V454 are conserved among all species analyzed and each have Polyphen2 scores of 1 (damaging) and SIFT scores of 0 (damaging). Each of the three FP mutations is annotated in public databases: 1000 Genomes (URL: http://browser.1000genomes.org) (Auton et al 2015); NHLBI Exome Sequencing Project (URL:

http://evs.gs.washington.edu/EVS); Exome Aggregation Consortium (ExAC), Cambridge, MA (URL: http://exac.broadinstitute.org). Minor allele frequency (MAF) was 0.43% for V454A variant, 0.08% for R723Q, and 1.5% for R276W (Table 4.2 and Table 4.3).

The high frequency of the variants found in our patients prompted our genetic screening of a cohort of 327 blood donors. Of note, our analysis demonstrated the presence of variant R276W in 0.3% of this cohort (1/327) and the absence of the other two mutations V454A and R723Q, consistent with the MAF values reported to date.

Table 4.2. Mutations found in FP patients

Family code	ABCB6 mutations	SNP ID	MAF[§]	PolyPhen-2/ SIFT scores	References
Bolivian	c.1361T>C; p.V454A*	rs61733629	0.001 (C)	0.996/0	*unpublished data*
Cardiff 2	c.826C>T; p. R276W # c.2168G>A; p.R723Q #	rs57467915 rs148211042	0.013 (T) 0.001 (A)	1/0 0.997/0	*unpublished data*
Irish	c.826C>T; p. R276W	rs61733625	0.013 (T)	1/0	*unpublished data*
Lille	c.1123 C>T; p. R375Q	Not annotated	-	1/0	*Andolfo I. et al., 2013*
Falkirk	c.1124 G>A; p.R375W	Not annotated	-	1/0	*Andolfo I. et al., 2013*
East London	c.1124 G>A; p.R375W	Not annotated	-	1/0	*Andolfo I. et al., 2013*

*****Mutations in homozygous state
[#] The two mutations are in trans (see results section for details)
[§]Overall minor allele frequencies estimated from public databases (1000 genomes, ESP6500:European_American, CORNELL:AGI_ASP_population)

Table 4.3. Minor allele frequency of the ABCB6 variants here identified

Database		MAF (C) rs61733629 (c.1361T>C; p.V454A)	MAF (T) rs57467915 (c.826G>T; p.R276W)	MAF (A) rs148211042 (c.2168G>A; p.R723Q)
1000 genomes				
	AFR	0/1322	1/1322	0/1322
	AMR	28/694	2/694	0/694
	EAS	1/1008	0/1008	0/1008
	EUR	0/1006	15/1006	1/1006
	SAS	0/978	1/978	0/978
	ALL	**29/5008; 0.58%**	**19/5008; 0.38%**	**1/5008; 0.02%**
NHLBI Exome Sequencing Project				
	ESP6500:European_American	2/8600	114/8600	9/8600
	ESP6500:African_American	2/4406	17/4406	2/4406
	ALL	**4/13006; 0.03%**	**131/13006; 1%**	**11/13006; 0.08%**
Exome Aggregation Consortium (ExAC)				
	ALL	**556/121256; 0.46%**	**632/33350; 1.9%**	**101/118464; 0.09%**
TOT (1000 genomes EUR+ESP6500:European_American+ ExAC)				
		618/144278; 0.43%	**782/51364; 1.5%**	**113/136478; 0.08%**

Minor allele frequency of the variants identified in this study by the analysis of the public databases 1000 genomes, NHLBI Exome Sequencing Project and Exome Aggregation Consortium

4.1.3 ABCB6 mutations produce conformational changes in model structures

To analyze potential consequences of the identified mutations on protein structure, we generated three-dimensional structural models of the (putatively dimeric) human WT ABCB6 residues 231- 10 827 and FP mutant polypeptides V454A, R276W, and R723Q (see Methods). Figure 4.1 shows 3D structural models of homodimeric WT ABCB6 in inward- and outward-facing conformations, highlighting sites of the homozygous and compound heterozygous FP missense mutations studied in this paper.

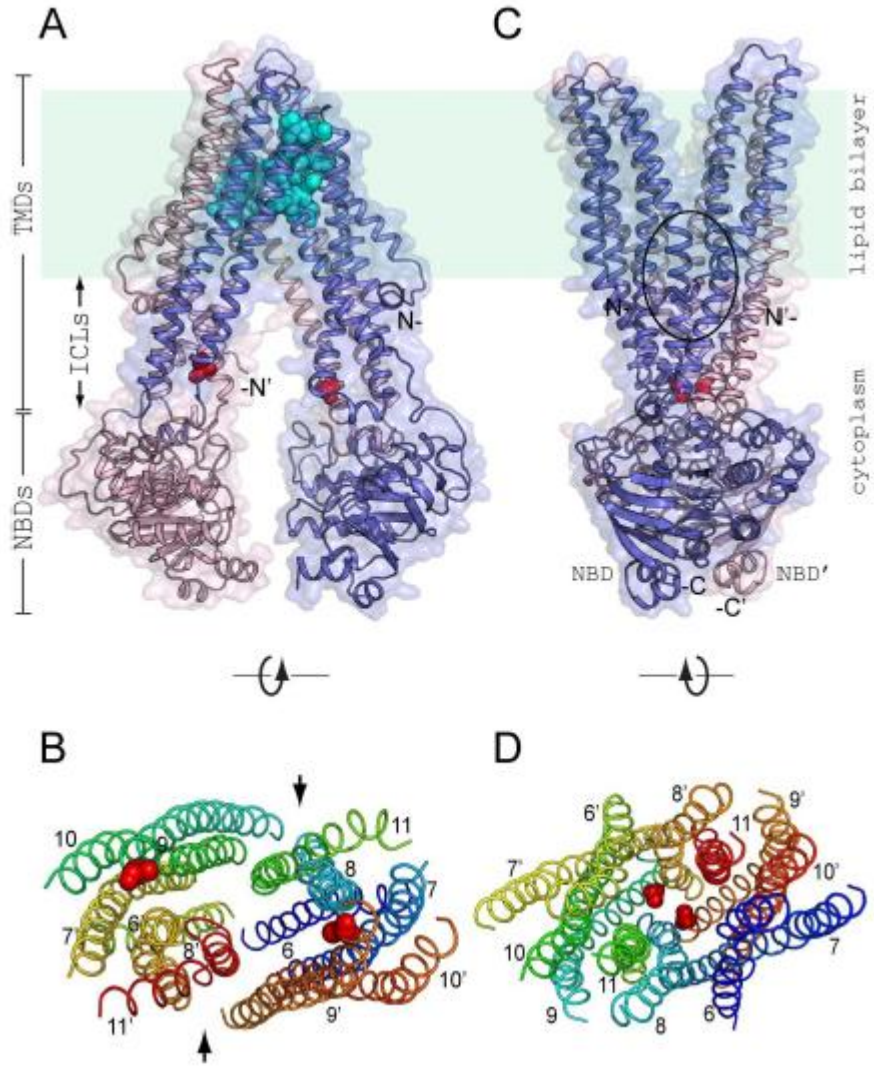

Figure 4.1. Three-dimensional structural model of human ABCB6 mutations

A. Three-dimensional structural model of a portion of homodimeric WT human ABCB6 in an inward-facing conformation, as modeled on the aligned structure of M. musculus ABCB1A (PDB ID 3G5U). Monomer "a" (blue) of the homodimer represents ABCB6 aa residues 246 (N-) to 826 (- C), modeled on transmembrane helices 1-6 and NBD-1 of ABCB1A. Monomer "b" (pink) of the homodimer represents ABCB6 aa residues 237 (N'-) to 826 (-C') modeled on ABCB1A transmembrane helices 7-12 and its NBD-2. A surface model is superposed on the modeled polypeptide backbone ribbon structure. DHSt homozygous mutation site V454 (red spheres) is located between the membrane-spanning helices and the NBDs, extending into the cytoplasmic vestibule of the dimer. Locations of

the compound heterozygous DHSt mutation sites R276 (magenta spheres)/R723 (olive spheres) are also shown. Arrows mark R276 of monomer A (located within the lipid bilayer) and R723 of monomer B (located within the NBD region in the cytoplasmic vestibule) of the dimer. The cavity (cyan spheres) at the intermonomeric interface outlines a postulated intra-membrane binding site for inhibitors of ABCB6-mediated porphyrin transport32, corresponding to the ABCB1 binding site of inhibitor QZ5933. In this and subsequent figures, each modeled ABCB6 monomer lacks its ectofacial N-terminal tail and putative transmembrane spans 1-5, but includes putative transmembrane spans 6-11 (TM) followed by the single nucleotide-binding domain (NBD). B. Transverse intra-membrane profile of the modeled inward-facing conformation of dimeric WT ABCB6 (as in panel A), with transmembrane helices rotated 90° around the axis shown. The view (lacking NBDs) looks outward from the ICL region, near the site of separated mutation site V454 (red) and farther from mutation site R276. The colored M1 domain helices are numbered 6-11 for ABCB6 monomer "a", and 6'-11' for the monomer "b" of the ABCB6 dimer. The arrows between helices 9 and 11 on one side, and helices 9' and 11' on the other side of the dimer mark the locations of side apertures proposed in mouse ABCB1 to mediate hydrophobic drug uptake from the inner leaflet of the lipid bilayer for subsequent efflux from the cell, or for flippase-like transfer to the outer leaflet33. C. Three-dimensional structural model of homodimeric WT human ABCB6 in an outward-facing conformation, as modeled on the aligned structure of S. aureus Sav1866 (PDB ID 2HYD). The black oval encloses a central cavity at the inter-monomeric interface, hypothesized to be an intra-membrane substrate binding site (as predicted for homodimeric Sav1866 of S. aureus34). Sites of homozygous and compound heterozygous mutations are shown using similar colored spheres as in panel A. D. Transverse intramembranous profile of the modeled outward-facing conformation of dimeric ABCB6 (as in panel C), with the transmembrane helices rotated 90o around the axis shown. The view (lacking 20 NBDs) looks inward from the extracellular edge of the outer leaflet of the membrane bilayer towards the approximated mutation sites V454 (at the level of the ICL region) and R276 (farther from the ICL region); color scheme as in panel C. Helices are labeled at ends closest to reader. The figure was prepared in PyMOL.

Transverse views of intra-membrane bilayer regions are also presented. Comparison of WT with mutant models reveals that these mutations cause detectable conformational changes in regions on or near the missense substitution sites and at several more remote locations. In inward-facing models of homodimeric FP mutant V454A, the presence of Ala decreased by 2.3 Å the WT Cα-Cα interatomic distance between chain a residue 454 and chain b residue 454. In contrast, this change was minimal in the outward-facing conformation. The WT loop structure at aa 362-367 (packed adjacent to chain b residue 454 in the inward-facing conformation) underwent a partial loop-to-helix transition in the homodimeric FP mutant V454A. Furthermore, the WT Cα-Cα interatomic distance between chain a residue 276 and remote chain b residue 723 decreased by 3.3 Å in the heterodimeric FP mutant R276W (chain a)/R723Q (chain b). The inward-facing conformation of this heterodimeric mutant also induced a loop-to-helix transition of chain a residues 408-409 at the ecto-end of a transmembrane helix and spatially adjacent to chain a missense substitution R276W. These amino acid substitutions also modestly alter interhelical distances near the mutation sites. Structural superposition of modeled WT polypeptide with each modeled mutant polypeptide reveals larger global structural deviations of mutant polypeptides in inward-facing than in outward-facing conformations (Table 4.4). Modeled heterodimeric

R276W/R723Q and homodimeric V454A mutant polypeptides exhibited greater structural deviation from WT than did homodimeric mutants R276W or R723Q (Table 4.4).

Table 4.4. RMSD (Å) of superposed homology-modeled structures of the indicated patient-derived mutant ABCB6 dimers with the modeled wildtype ABCB6 homodimer

Mutant ABCB6	Inward-facing	Outward-facing
V454A/V454A	1.48	0.81
R276W[a]/R723Q[b]	1.88	0.58
R276W[b]/R723Q[a]	1.57	0.74
R276W/R276W	0.98	0.29
R723Q/R723Q	1.17	0.79

4.1.4 ABCB6 mutations cause no alteration of expression and cellular localization

We modeled *in vitro* our patients' genotypes by transient transfection of WT and mutant ABCB6 expression plasmids into HEK293 cells. No significant differences between mutant and WT mRNA accumulation were evident 72h post-transfection (Figure 4.2A). Similarly, immunoblot analysis of heterologous FLAG tag confirmed equivalent accumulation of WT and mutant heterologous ABCB6 polypeptides (Figure 4.2B).

We also tested effects of the mutations on ABCB6 membrane localization. Confocal microscopy analysis showed that all mutant polypeptides were expressed predominantly at the HEK-293 cell peripheral membrane, as demonstrated by colocalization of ABCB6-FLAG with the membrane marker lectin WGA wheat germ agglutinin (Figure 4.2C).

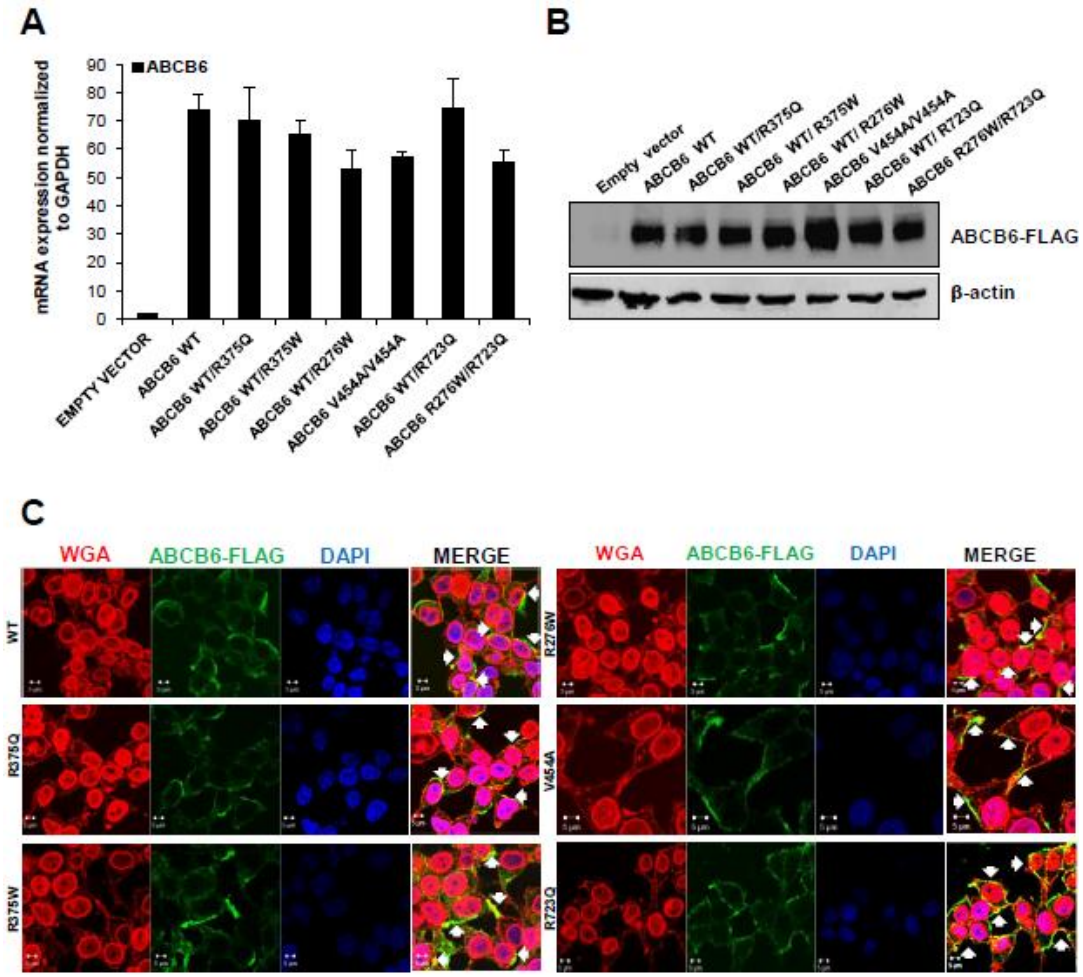

Figure 4.2. Expression and localization of ABCB6 mutants.
A. ABCB6 mRNA levels in HEK-293 cells transfected with ABCB6 WT and mutants and empty vector as control. Values are means +/- s.e.m. of three independent experiments. *p < 0.001 WT, WT/R375Q, WT/R375W, WT/R276W, V454A/V454A, WT/R723Q, R276W/R723Q vs empty vector. B. Immunoblot showing ABCB6 Flag protein expression in HEK-293 cells transfected with FLAG tagged WT or mutant ABCB6 variants, or with empty vector as control and GAPDH as loading control. One of two similar experiments. C. Laser-scanning confocal microscopy images of HEK-293 cells transfected with WT or mutant ABCB6 variants, or with empty vector as control, analyzed by immunofluorescence with rabbit polyclonal anti-ABCB6 antibody (green) and WGA (membrane marker, staining both the nuclear envelope and the plasma membrane, red), with merged signal showing regions of colocalization in yellow (white arrows indicate the yellow regions in the merge). Cells were imaged with a Zeiss LSM 510 meta confocal microscope equipped with a 1.4 NA oil immersion plan Apochromat 100× objective. Intensity and contrast were adjusted with Axiovision software. Representative of three independent experiments.

4.1.5 ABCB6 mutation R276W increases potassium efflux from red blood cells of a blood donor

A blood sample from the blood donor heterozygous for ABCB6 variant and samples from two control donors were obtained and stored four weeks at 4°C under blood banking conditions. Extracellular and intracellular potassium levels were measured throughout the storage period. As shown in Figure 4.3A the

potassium efflux of blood donor after 28 days of storage is about 3.5 fold higher than the controls. Correspondingly, the intracellular RBCs potassium content is about 2.5 fold lower than the controls (Figure 4.3B). The degree of hemolysis over time for the blood samples was evaluated during storage by measurement of free Hb levels and was the same for three samples (data not shown). The data demonstrated that the physiological consequences of the blood donor's mutation is potassium efflux higher than in controls, and similar to that observed in FP patients. Moreover, immunoblot analysis on RBCs from the blood donor carrying R276W mutation demonstrated that the expression of ABCB6 does not differ between mutated donor and healthy controls (Figure 4.3A).

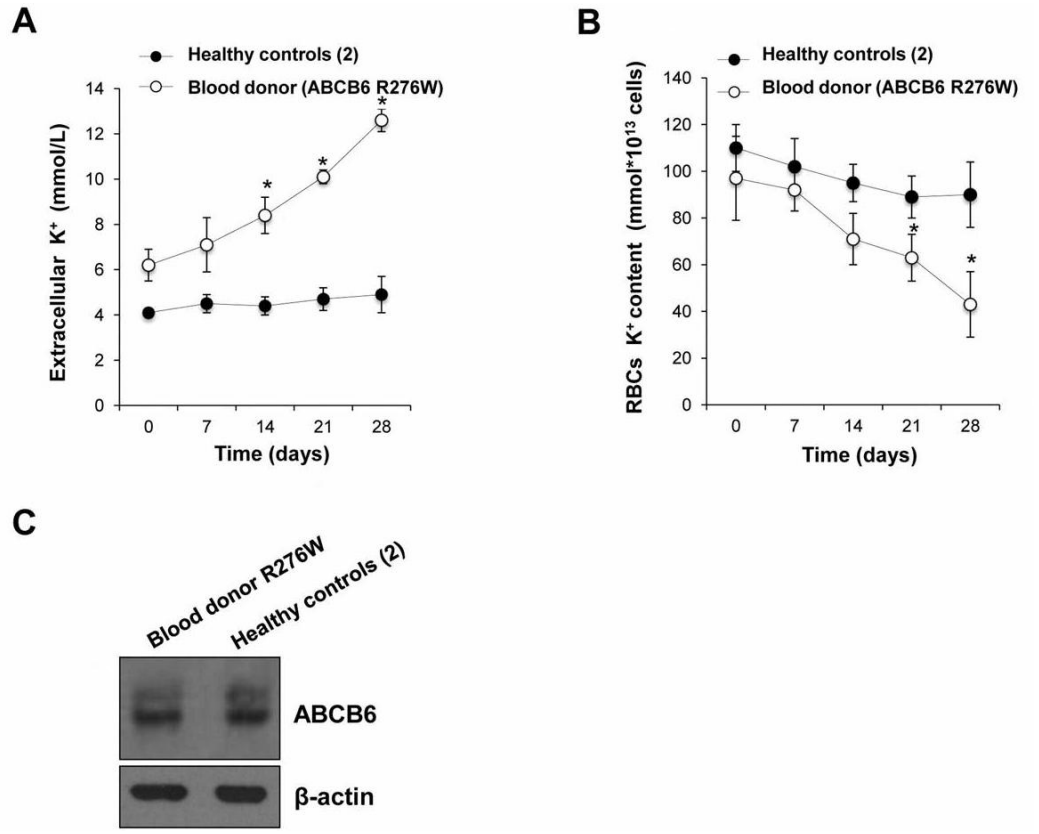

Figure 4.3. ABCB6 protein expression and potassium efflux in red blood cells of blood donor carrying ABCB6 R276W variant.

A. Plasma K content (expressed as mmol/L of whole blood) of blood from donor heterozygous for ABCB6 mutation R276W and from two healthy controls after 0D, 7D, 14D and 28D cold storage under blood banking conditions. * $p < 0.01$ donor vs two healthy controls. B. Intracellular K content (expressed as mmol/10^{13}cells) of blood from donor heterozygous for R276W and from two healthy controls after 0D, 7D, 14D and 28D cold storage as in A. Ion contents in A and B were measured by atomic absorption spectrometry, and represent means +/- s.e.m. of 3 independent experiments. * $p < 0.01$ donor vs two healthy controls . C. Immunoblot showing ABCB6 protein expression in RBC membranes from blood donor heterozygous for mutation R276W and pooled membranes from two healthy controls. β-actin was used as loading control. One of three similar experiments.

4.1.6 ABCB6 mutations cause cation flux alterations

We next evaluated cell potassium content in HEK-293 cells over-expressing WT ABCB6 and different ABCB6 mutant variants. Preliminary experiments comparing cells maintained for 8h at 37°C or 30°C revealed no differences (data not shown). To mimic shipping conditions (critical for the serum [K+] alteration observed in the FP patients) we exposed HEK-293 cells over-expressing WT or mutant ABCB6 variants to 0.12 g rotary shaking at 30°C for 8 h. As shown in Figure 4.4A, levels of extracellular K in media from HEK-293 cells over-expressing mutant ABCB6 variants were significantly higher than for cells expressing WT ABCB6. Correspondingly, residual intracellular Rb content was significantly reduced in cells expressing three of the ABCB6 mutant genotypes, WT/R375Q, WT/R375W, V454A/V454A, as well as in the double mutant R276W/R723Q, compared to either WT ABCB6 or the other ABCB6 variants (WT/R273Q, WT/R276W) (Figure 4.4B). These data show different impacts of individual ABCB6 mutations on cellular K+ efflux insensitive to ouabain plus bumetanide, and an incrementally increased effect on cell K+ efflux of coexpression of the compound heterozygous ABCB6 mutations R276W/R723Q.

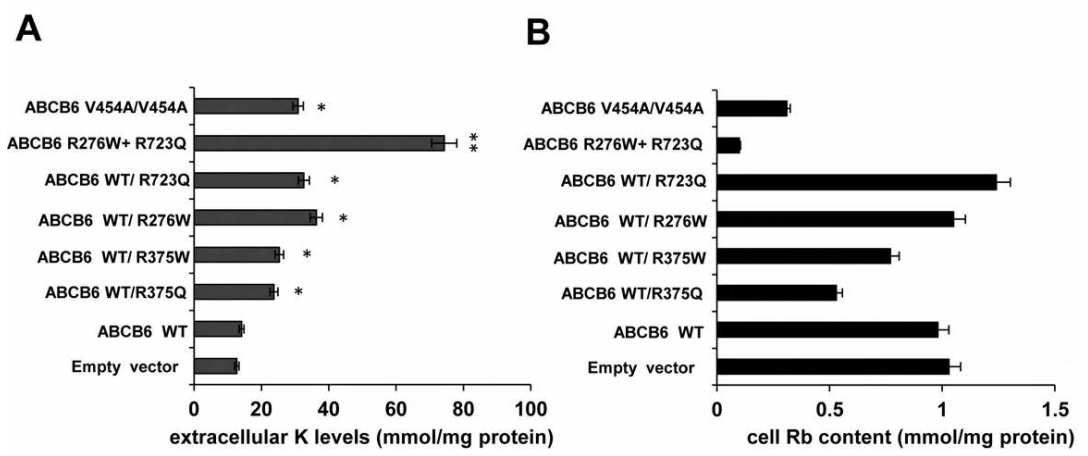

Figure 4.4. Analysis of potassium efflux of ABCB6 mutants.
A. K content of extracellular medium sampled from cultures of cells overexpressing ABCB6 WT or ABCB6 FP mutants. Ion contents measured by atomic absorption spectrometry were expressed as mmol/mg protein. **p < 0.001 R276W/R723Q vs empty vector and WT; *p < 0.05 for WT/R375Q, WT/R375W, WT/R276W, V454A/V454A, WT/R723Q vs WT. B. Rb content of cells overexpressing ABCB6 WT and ABCB6 FP mutants, expressed as mmol/mg protein. Values in A and B are means +/- s.e.m. of four independent experiments.

4.2 KCNN4 gene identification as causative of DHS

4.2.1 Cases report

Proband II.3 from family NA, a 40-year-old Italian woman, was referred to the Medical Genetics service of University of Naples “Federico II” for moderate macrocytic anemia. She was born at term after an uncomplicated pregnancy to healthy non-consanguineous parents. Birth parameters were normal, and neonatal jaundice was treated with routine phototherapy. At the age of 7 years, she was referred for severe anemia after an acute tonsillitis. No transfusions were required. Blood examinations showed macrocytic anemia, with high indirect bilirubin and LDH, and negative Coombs test. Subsequent Hb levels remained <11 mg/dl, and hemolytic anemia was suspected. Measurement of red cell survival showed reduced lifespan with intra-marrow and intra-splenic hemolysis. Bone marrow revealed erythroid hyperplasia and dyserythropoiesis, leading to suspicion of atypical hereditary spherocytosis. At 21 years of age, the patient underwent splenectomy and cholecystectomy without improvement in her anemia. She remained transfusion-independent through two pregnancies with caesarean deliveries. The first pregnancy was complicated by fetal distress. The first male son (III.1) was born at term with normal birth parameters and jaundice with bilirubin levels of 21 mg/dl, treated with phototherapy for 7 days. Blood examinations showed normocytic anemia (Hb 9.2 g/dl) and thrombocytopenia. Echocardiography showed pulmonary stenosis and patent ductus arteriosus. Persistent normocytic anemia was observed in infancy. His persistent hemolysis resembled that of his mother. Mother (II.3) and son (III.1) were jointly referred to our Medical Genetics Unit for diagnostic assessment at the respective ages of 40 and 10 years. At physical examination, they presented jaundiced skin and sclerae with hepatomegaly. The male son (with mild intellectual disability and learning problems) had splenomegaly of 13 cm and cholelithiasis evident on ultrasound. Blood examination showed moderate macrocytic anemia with reticulocytosis in the mother and mild normocytic anemia in the child. Osmotic fragility and eosin-5-maleimide (EMA) binding were normal in both patients. Plasma [K+] after overnight storage at 48C was not increased in either III.1 or II.3 as compared to healthy controls. Complete blood count data are shown in Table 4.5.

Table 4.5. Biochemical and hematological data of index cases from both families

Parameters	Normal range	Family NA-II.3[#]		Family NA-III.1	Family WO-IV.5	Family WO-III.5
		pre-	*post-*			
Age (years)	-	13	40	10	21	56
Hb (g/dL)	11.5-16.5	10.4	9	10.5	12.5	13.3
RBC (10^6/µL)	3.8-5.8	3.0	2.5	3.6	3.3	3.9
Hct (%)	37-47	30.5	28.5	31.3	35.6	37.0
MCV (fL)	76-96	101	112	86	96	103
MCH (pg)	27-32	34.3	35.4	28.8	33.7	-
MCHC (g/dL)	30-35	34	31.6	33.5	36.1	-
RDW (%)	11.5-15.5	-	14.5	4.1	14.7	-
Retics %	0.5-2	11.8	17.7	6.3	12.2	6.5
Retics abs count (x10^3/µL)	-	358	450	229	403	254
PLT (10^3/µL)	150-400	-	841	184	195	250
WBC (10^3/µL)	4-11	5.0	8.8	6.4	7.3	9.5
Ferritin (ng/mL)	15-233	-	580	132	450	-
Transferrin (mg/dL)	200-360	-	158	217	-	-
Serum iron (µg/dL)	37-145	-	230	127	-	-
Transferrin saturation (%)	15-45	-	-	41	-	-
Total bilirubin (mg/dL)	0-1.2	3.88	4.3	4.7	12.1	1.7
Conjugated bilirubin (mg/dL)	0-3	0.55	0.7	0.5	-	-
Unconjugated bilirubin (mg/dL)	<1	3.33	3.6	4.1	10.9	1.5
LDH (IU/L)	240-480	-	260	579	650	280
Haptoglobin (g/L)	0.5-3.2	-	<0.298	<0.298	<0.2	-
HbA2 (%)	2-3.4	1.8	1.8	2.8	2.5	-
HbF (%)	<1	0.8	0.8	0.8	1.1	-
K (mmol/L)	3.5-5.3	-	4.5	3.8	4.8	4.5
Ca (mg/dL)	8.9-10.3	-	10.3	10.1	9.8	10.2

Splenectomized at age 40

Peripheral blood smear of patient II.3 after splenectomy revealed several stomatocytes and anisopoikolocytosis; patient III.1 showed rare stomatocytes and anisopoikolocytosis (Figure 4.5A). Red cell ektacytometric analysis of post-splenectomy patient II.3 showed a slight decrease of DiMax and Omin, with a slight right-shift. Patient III.1 showed a left-shifted curve indicating dehydration as usual for DHSt patients (Figure 4.5B). Patients in family WO exhibited well-compensated anemia with normal or near-normal hemoglobin levels and markedly increased reticulocytes. The osmotic gradient ektacytometry curve was left shifted. The deformability index remained within the normal range and O' and Omin points were left-shifted as compared to the previously described DHS families harboring PIEZO1 gain-of function mutations.

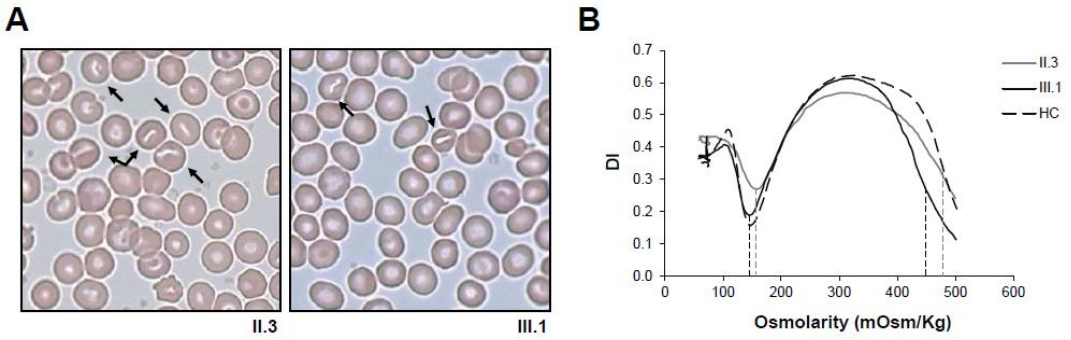

Figure 4.5. Clinical and functional analysis of the KCNN4-R352H mutation.
A. Peripheral blood smear examination of patients II.3 (post-splenectomy) and III.1 showed marked anisopoikolocytosis, with stomatocytes (arrows). B. The red cell deformability index (DI) was measured as a function of increasing bath osmolality in control red cells (dotted line) and red cells from III.1 (solid black line) and II.3 (solid gray line). Omin (dotted line on the left) represents the osmolality at which red cells are maximally swollen. O' (dotted line on the right) indicates the osmolarity at which DI is half-maximal. The ektacytometry profile of II.3 (after splenectomy) shows diminished DImax; that of III.1 shows a left-shifted curve indicating deydratation.

4.2.2 KCNN4 mutational analysis

We performed WES analysis in both families presenting with clinical suspicion of DHS but without cosegregating *PIEZO1* mutations. Affected subjects II.3 and III.1 of the family NA revealed, the heterozygous missense mutation c.1055G>A, p.R352H (Figure 4.6A). This mutation was absent in the three unaffected subjects of the same family. This mutation occurred in a codon containing a CpG dinucleotide (ttcCGCcag), probably a mutational 'hot spot'. The mutation was a de novo event in proband II.3, as it was absent in both parents (I.1 and I.2). In family WO, previously described in linkage with Chr.16 (Vantyghem et al 1991), we found the novel, heterozygous missense mutation c.844G>A, p.V282M. In this multigenerational family, we also extended analysis to additional affected subjects, confirming the segregation of the mutation (Figure 4.6B), which was absent from unaffected family members. Both of the reported *KCNN4* mutations have Polyphen-2 score 1 (damaging) and SIFT score 0 (damaging). Neither mutation was found in the 1000 genomes database.

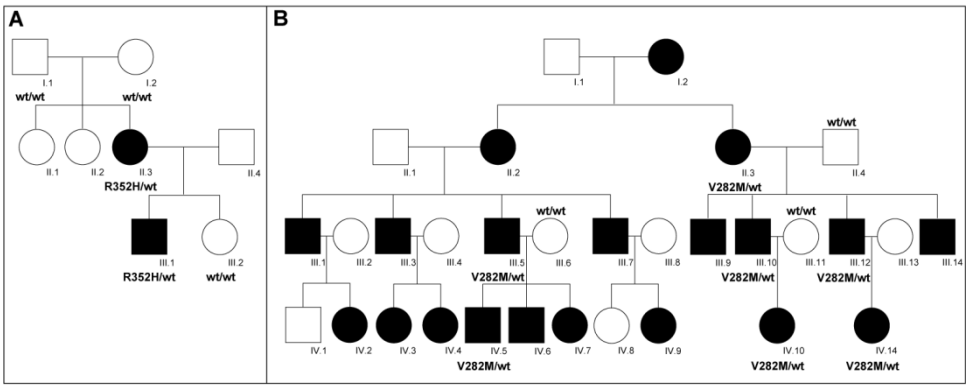

Figure 4.6. KCNN4 mutations
A. Inheritance pattern of KCNN4-R352H mutation in the Italian family (NA). The mutation is a de novo event in propositus II.3. B. Inheritance pattern of KCNN4-V282M mutation in the American family (WO).

4.2.3 Red cell membrane proteins in patients with KCNN4 mutations

KCNN4 mRNA levels were unaltered in Family NA, as evaluated by qRT-PCR (Figure 4.7A). We further evaluated expression levels of several erythrocyte membrane proteins involved in other RBC defects, including band3 (AE1), ABCB6, PIEZO1 and EPB72. These were unaltered except for apparent reductions in PIEZO1 in affected subjects II.3, III.1 and in unaffected subject I.1 (Figure 4.7B).

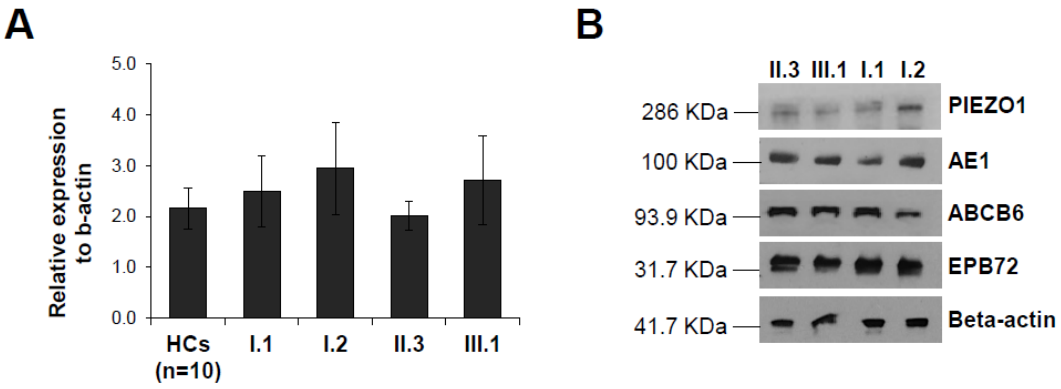

Figure 4.7. Characterization of KCNN4 and other RBCs gene products in family NA.
A. KCNN4 mRNA level normalized to b-actin. No differences in KCNN4 expression of II.3 and III.1 patients compared to healthy controls (HCs, 2.260.4; II.3, 2.060.3, P50.85; III.1, 2.760.9, P50.59) were observed. Data are presented as mean6SE of 3 experiments. P value has been calculated by Student t test. B. Immunoblot showing protein expression of PIEZO1, AE1, ABCB6, and EBP72 in human red blood cell membrane (80 µg) from patients II.3 and III.1 and unaffected family members I.1 and I.2. Beta-actin is the loading control. One of three similar experiments.

4.2.4 KCNN4 during erythroid differentiation and mouse embryogenesis

To investigate the role of KCNN4 in erythroid cells, we first examined KCNN4 expression in an ex vivo model of erythroid differentiation. CD34+ cells isolated from the peripheral blood of healthy volunteers were induced to erythroid differentiation by 7 and 14 days of erythropoietin treatment, as detailed in Materials and Methods. As shown in Figure 4.8A, KCNN4 mRNA was significantly increased after 14 days of erythropoietin treatment ($p = 0.002$ for the trend). The same trend was observed in K562 cells induced to erythroid differentiation with hemin for 4 and 6 days ($p = 0.01$ for the trend) (Figure 4.8B). We further analyzed Kcnn4 expression during mouse embryonic development. We collected mouse embryos at E9.5, E10.5, E12.5, E15.5 for qPCR analysis of murine KCNN4 expression. Kcnn4 mRNA abundance increased gradually from E9.5 to E15.5 ($p = 0.0002$; Figure 4.8C).

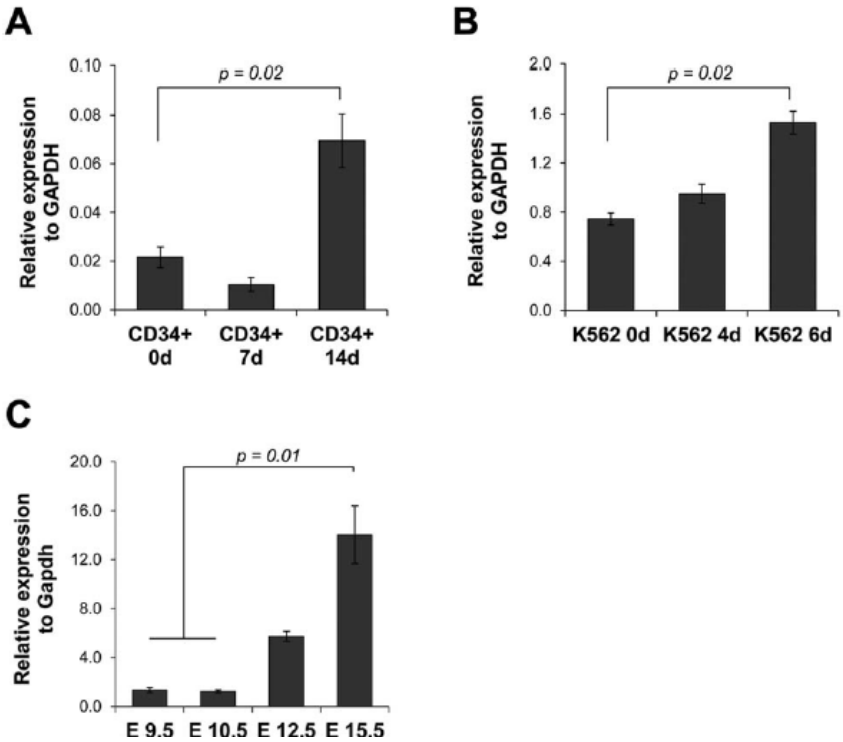

Figure 4.8. KCNN4 expression profiling during human erythroid differentiation and mouse embryonic development.

A. KCNN4 mRNA levels (normalized to GADPH) in CD341 cells induced to erythroid differentiation by EPO at 0, 7 and 14 days. **B**. KCNN4 mRNA levels (normalized to GADPH) in K562 cells induced to erythroid differentiation by hemin at 0, 4 and 6 days (n536SE of 3). **C.** KCNN4 mRNA levels (normalized to GAPDH) in whole murine C57BL/6 embryos at E9.5, E10.5, E12.5, and E15.5. All P values are by Student T-test.

4.3 Modifier effects of PIEZO1 variant on DHS phenotype

4.3.1 Cases report

The case 1 is a 42 male years old form Jersey island that suffers from hemolytic anemia for over 20 years. Four of his five children also suffer from anemia (Figure 4.9).

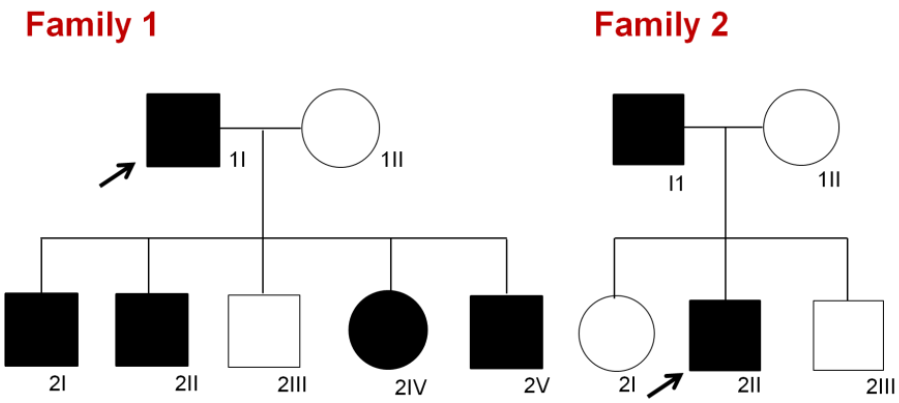

Figure 4.9. Partial pedigree of the two families here analyzed.
Left panel. Inheritance pattern of PIEZO1-E2492_L2493dup mutation in the family 1. The proband 1I is indicated by the arrow. **Right panel**. Inheritance pattern of PIEZO1-E2492_L2493dup mutation in the family 2. Proband 2II (indicated by the arrow) carried also the mutation R1864H in PIEZO1.

He shows iron overload (negative for hemochromatosis), gallstones and splenomegaly with normal liver function. CBC shows decreased hemoglobin levels, increased MCV, MCHC and reticulocytes count (Table 4.7).

Table 4.7. Blood count and laboratory data of the probands

	Proband 1	Proband 2	Normal range
Age (years)	42	5	
Complete blood count			
RBC (10^6/µL)	5.1	3.47	4.2-5.6
Hb (g/dL)	9.5	9.1	12-17.5
MCV (fL)	99	25.7	80-97
MCHC (g/dL)	39.7	26.2	32-38
Ret (%)	15	9.5	0.5-2
Laboratory data			
Total bilirubin (mg/dL)	9.6	3.9	0.2-1.1
Serum iron (µg/dL)	234	28	45-150
Ferritin (ng/mL)	646	55	5-150

Moreover, he shows high levels of bilirubin, serum iron and ferritin, trasferrin indicating iron overload saturation and LDH. The examination of peripheral blood

smear highlighted the presence of macrocytosis, polychromasia, schistocytes and some stomatocytes . The case number 2 is a child of ten years old. He present anemia from the birth. CBC shows decreased hemoglobin levels, normal MCV, elevated reticulocytes count (Table 4.7). He shows, gallstones and splenomegaly with high levels of bilirubin. The examination of peripheral blood smear highlighted the presence of polychromasia, schistocytes and some stomatocytes

Ektacytometric analyses were performed for all the subjects here analyzed. As we can see, the curves showed a leftward shift of the bell-shaped curve for all the patients in respect to the healthy controls indicating dehydration of the RBCs (Figure 4.10).

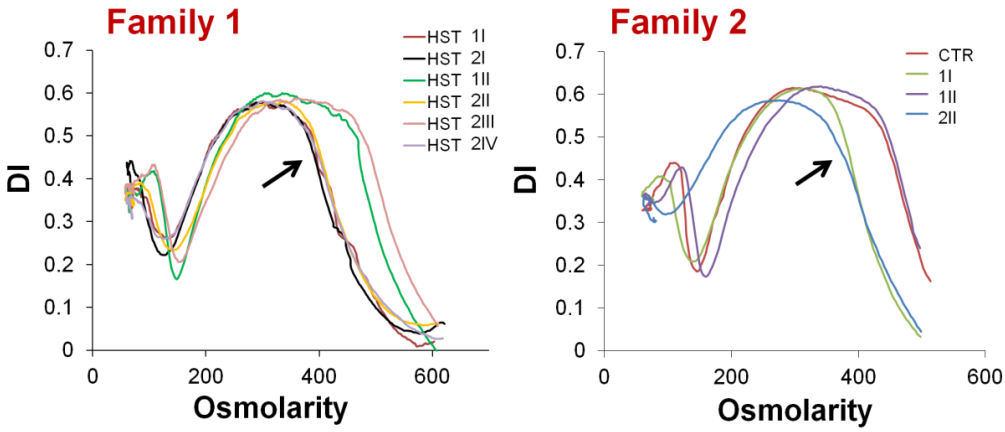

Figure 4.10. Ektacytometry analyses of the two families here analyzed.
Panel on the left. The red cell deformability index (DI) was measured as a function of increasing osmolarity red cells from family 1 patients 1I, 2I, , 2III, 2IV and internal healthy controls of the same family. **Panel on the right.** The red cell deformability index (DI) was measured as a function of increasing osmolarity red cells from family 2 patient 2II and from healthy controls of the same family 1I, 1II, and from a healthy control.

4.3.3 PIEZO1 mutational analysis

We sequenced *PIEZO1* gene in both families presenting with clinical suspicion of DHS. Affected subjects of family 1 revealed, the heterozygous missense mutation c.7473_7478dupGGAGCT, p.E2492_L2493dup. This mutation was absent in the unaffected subjects of the same family. In family 2, we found the same duplication present in the family 1, but also an additional PIEZO1 mutation p.R1864H. The analysis of inheritance pattern in the proband of family 2 showed that Arg1864His is a *de novo* mutation. Cloning experiments showed the presence of both mutations E2492_L2493dup and R1864H *in cis* in the proband of family 2.

4.3.4 PIEZO1 expression analysis

We modeled *in vitro* our patients' genotypes by transient transfection of WT and mutant PIEZO1 expression plasmids into HEK293 cells. No significant differences between mutant and WT *PIEZO1* mRNA were evident 72h post-transfection (Figure 4.11A). Similarly, immunoblot analysis of PIEZO1 confirmed equivalent expression of WT and mutant PIEZO1polypeptides (Figure 4.11B).

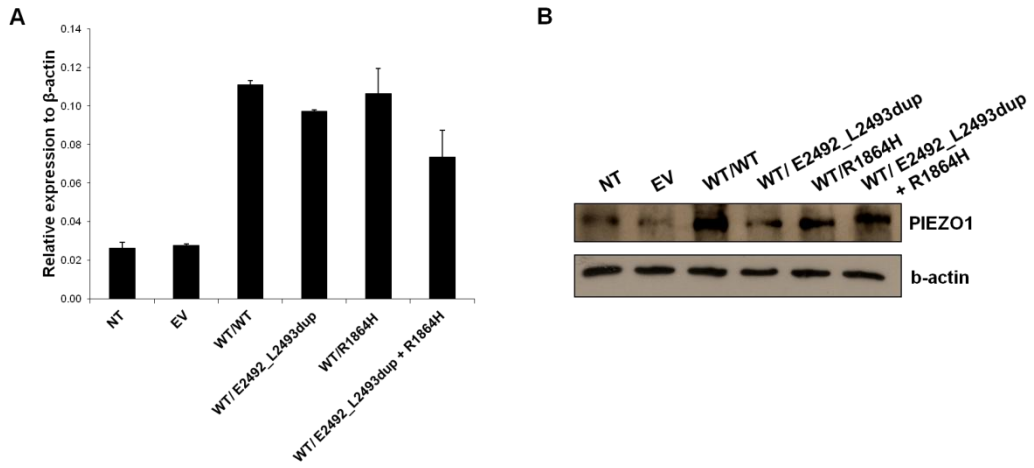

Figure 4.11. Expression levels of PIEZO1 in Hek293 cells transfected with the mutants constructs.
Panel A. PIEZO1 mRNA levels in cells over-expressing human PIEZO1 WT, PIEZO1 Glu2492_Leu2493dup, PIEZO1 Arg1864His. Values are means +/- s.e.m. of three independent experiments. **Panel B.** Immunoblot showing PIEZO1 protein expression in cells over-expressing human PIEZO1 WT and mutants. β-actin is loading control. One of two similar experiments.

4.3.5 Cation flux in PIEZO1 mutants

Measurement of ouabain- and bumetanide-resistant net cation flux demonstrated a greater loss of cell K from both mutants PIEZO1-expressing cells than from WT PIEZO1-expressing cells (Figure 4.12). Of note, the presence *in cis* of both the mutations causes an increase of potassium efflux compared to the only E2492_L2493dup.

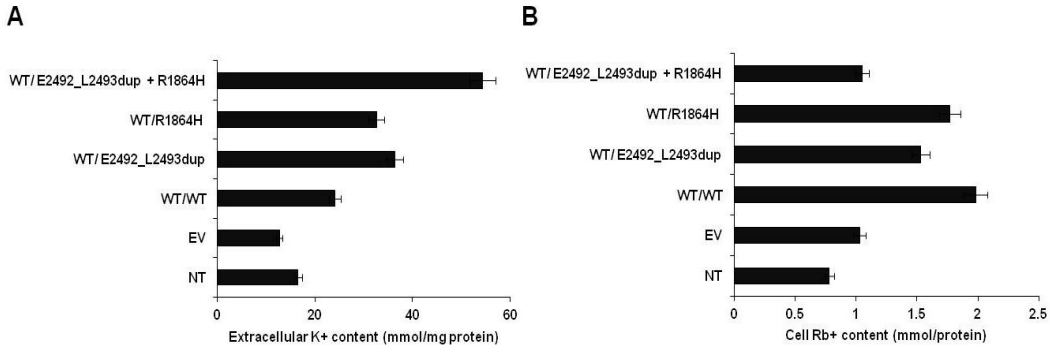

Figure 4.12. **Panel A.** Cell Rb+ content of cells over-expressing CDS of PIEZO1 WT and mutants (* p value <0.05 WT vs EV; ** p value <0.001 R1864H and E2492_L2493dup vs WT). **Panel B.** Extracellular K+ content in culture medium of the same cells described in B (* p value <0.05 WT vs EV; ** p value <0.001 R1864H and E2492_L2493dup vs WT). Values are means +/- s.e.m. of 3 independent experiments.

5. Discussion

This work take together three studies on three different ionic channels, all involved in the pathogenesis of erythrocyte defects caused by alterations in membrane transport.

In this study we have reported three new mutations in the FP-disease gene *ABCB6*. FP had been described previously as a dominant condition, but, for the first time, we report two FP patients with homozygous or compound heterozygous mutations, both novel patterns of inheritance for FP. Of note, those patients homozygous and compound heterozygous for ABCB6 mutations showed higher plasma [K+] than heterozygous patients. Moreover, the compound heterozygous also exhibited a value of MCV higher than in other patients. FP inheritance patterns thus constitute a crucial part of patient diagnostic evaluation.

ABCB6 variations are more common that previously predicted, as also reported for Lan- blood group carriers with *ABCB6* nonsense mutations causing the ABCB6-null RBC phenotype. Koszarska and colleagues showed that screening of erythroid ABCB6 expression reveals an unexpectedly high frequency of Lan mutations in healthy individuals (Koszarska et al 2014). Indeed, in public databases (1000 Genomes, NHLBI Exome Sequencing Project, Exome Aggregation Consortium) allele frequencies are 0.43% for V454A, 0.08% for R723Q and 1.5% for R276W. Moreover, the high frequency of ABCB6 variations in FP, including two FP patients found in a Cardiff blood donor cohort as recently described by Bawazir et al has clinical implications for blood transfusion screening and practice (Bawazir et al 2014). Our own screening of 327 blood donors of different geographical and ethnic origin corroborates this observation, with the R276W mutation found in 0.3% of our cohort. Our analysis of potassium efflux from blood donor RBCs under blood banking storage conditions confirmed the cation leak as shown by FP patients. Refrigerated storage of blood of FP patients causes rapid loss of potassium, and the extracellular potassium content of bags of stored cells increases during storage. This is of little consequence for the majority of transfusions, since the total amount of potassium transfused is relatively small compared to the total blood volume of the recipient. In contrast, this extracellular potassium can have serious or fatal consequences for neonates and infants receiving whole blood transfusions of large volume proportionate to body size. Several such cases of whole blood transfusion in infants leading to cardiac arrest and death have been described (Hall et al 1993; Chen et al 1999; Baz et al 2002; Smith et al 2008; Lee et al 2014).

The ABCB6 FP mutants overexpressed in HEK-293 cells showed no difference in accumulation of mRNA or protein, or in peripheral membrane immunolocalization as compared to WT ABCB6, and as previously demonstrated for ABCB6 FP variant R375Q. Consistent with these findings, *in silico* modeled 3D structures of these mutant ABCB6 polypeptide dimers predicted modest structural alterations of transmembrane and cytosolic ATP binding domains in both inward- and outward-facing conformations. Prediction of the consequences of these structural alterations to the cation leak process remain uncertain, since the relationship between the mutant cation leak and the (proposed but still debated) wild-type transport of porphyrins remains poorly understood. Future molecular dynamics simulation studies in a model lipid bilayer across microsecond time-scales will extend our understanding of the impact of these FP mutants on the structure, and possibly the function, of ABCB6.

To further characterize the role of ABCB6 mutants, we tested the hypothesis that their expression could modify K+ transport in HEK-293 cells in a manner similar to the altered K+ efflux in FP RBC. We found that cells expressing each mutant variant tested exhibited increased potassium efflux compared to WT. Co-expression in HEK-293 cells of the two mutant variants expressed by patient Cardiff in compound heterozygous form produced the highest value of potassium efflux among all tested mutants. These data demonstrated that the new mutations, whether homozygous or compound heterozygous, act at the cellular level as gain-of-function mutations.

Among ABC proteins, only the cystic fibrosis transmembrane regulator CFTR/ABCC7 itself is known to mediate ion channel function. However, several ABC proteins, in addition to CFTR, function as ion channel regulators (Higgins et al 1995; Welsh et al 1992; Inagaki et al 1995), including the Kir6 KATP channel regulatory subunits, sulphonylurea receptors SUR1, SUR2A, and SUR2B31. The question remains whether ABCB6 FP mutant polypeptides generate intrinsic cation leak pathways in membranes of RBCs (or experimentally in HEK-293 cells), or might secondarily dysregulate one or more endogenous membrane cation permeability pathways in erythrocytes (or HEK-293 cells). The negative results obtained to date in our electrophysiological studies conducted in HEK-293 cells and Xenopus laevis oocytes expressing WT or mutant ABCB6 variants (not shown) encourage further consideration of dysregulated endogenous electroneutral (or low-level electrogenic) transporters as cation leak mediators in FP red cells or cell models of heterologous expression.

Regarding DHS a recent study has highlighted a novel DHS gene, *KCNN4*, encoding the widely expressed KCa3.1 Gardos channel, a Ca21-sensitive K1 channel of intermediate conductance (Rapetti-Mauss et al 2015). We have presented here two additional DHS families with KCNN4 missense mutations, family NA with the recently described R352H mutation, and family WO with the novel mutation, V282M. Of note, the R352H mutation in family NA was a de novo event in patient II.3. We speculate that R352H could be a mutational hot spot, as it shares a typical CpG sequence, in which C>T and G>A mutations likely reflect deamination of methylated cytosine.

The mild hemolytic anemia and elevated reticulocyte counts in the families described here presented with a milder phenotype than exhibited by the two recently described DHS families with the KCNN4 R352H mutation. The first patient described by Mauss et al presented with severe in utero anemia, requiring one in utero transfusion at gestational week 27 and three additional perinatal transfusions, with mild anemia and splenomegaly present at 4 years of age. The other previously described patient had moderate, transfusion-independent chronic hemolytic anemia from early childhood onward, and underwent a cholecystectomy. DHS caused by PIEZO1 mutations has also been associated with wide variation in clinical phenotype. Several modifier genes could affect the phenotype of DHS patients, including PIEZO1. Indeed, patients II.3 and III.1 exhibited several PIEZO1 polymorphisms that might contribute to differences in their clinical phenotypes. Of note, splenectomy is contraindicated in PIEZO1-associated DHS because it is associated with severe thromboembolic events (Andolfo et al 2016). In contrast, splenectomy seems neither to predispose to thrombotic events nor to improve anemia in the small number of DHS patients reported to date with KCNN4 mutations. We speculate that in PIEZO1-associated DHS patients, the presence of the mutated channel, also involved in cell–cell adhesion processes (McHugh BJ et al 2012; McHugh BJ et al 2010), might predispose to RBC aggregation with a reduced threshold for thrombus formation. Our patients showed changes in ektacytometry parameters similar to those of PIEZO1-associated DHS patients. Family WO showed a curve more left-shifted than Family NA, demonstrating greater dehydration potentially attributable to the distinct consequences of the two missense mutations The solvent-accessible KCNN4 R352 is modeled within the CaMBD2a section (aa 344-353) of the multi-site calmodulin binding domain, within electrostatic interaction distance of calmodulin E84 and of E363 of the adjacent KCNN4 protomer. Ca2+ ligation by KCNN4-bound calmodulin increases open

probability of the KCNN4 K+-selective channel pore to increase K1 efflux from the red cell. Engineered mutation of KCNN4 R352 to Cys moderately prolongs the channel inactivation time constant without substantial change in activation time constant (Andolfo et al 2015). Indeed, the KCNN4 R352H mutation found by Rapetti-Mauss et al. in two DHSt families displayed increased K1 channel activity secondary to 10-fold increased Ca2+-sensitivity and to delayed channel inactivation. The KCNN4 V282 residue mutated in family WO is modeled near the C-terminal cytoplasmic end of transmembrane span S6 of the pore-forming domain, suggested to both line the cytoplasmic-facing pore lumen below the P-loop selectivity filter, and to contribute to channel activation. V282 is predicted to lie at the narrowest point of the pore vestibule below the selectivity filter, and is evolutionarily conserved as far back as the *D. melanogaster* Shaker K1 channel. The engineered KCNN4 mutation V282W shortened the channel's activation time constant without effect on the deactivation time constant, while also modestly increasing channel sensitivity to activation by intracellular [Ca++] (Bailey et al 2010). Engineered substitution of V282 with hydrophilic residues locked the channel in the open state (Garneau et al 2010). Thus, the properties of engineered mutations in each of the two alleles found independently mutated in our two DHS families are consistent with predicted gain-of-function properties of the DHS-associated KCNN4 mutations. However, neither of our DHS families exhibited pseudohyperkalemia, consistent with the previously described patients with KCNN4 R352H mutations (Rapetti-Mauss et al 2015). Biochemical data and T2* magnetic resonance indicate the presence of hepatic iron overload, previously described as an important complication of DHS (Andolfo et al 2016). This feature in a splenectomized patient further supports the role of dyserythropoiesis as reported for PIEZO1 mutation-associated DHS. KCNN4 expression gradually increased during erythroid differentiation of CD34+ cells and K562 cell lines, consistent with some role in erythroid maturation. Kcnn4 expression also increased during mouse embryonic development, possibly linked to its functions in many non-erythroid tissues, including the immune system, gut, bone, endothelial cells, heart, placenta, and pancreas (Maher et al 2003). Moreover, KCNN4 expression also increases during in vitro erythroid differentiation of murine ES cells (Vandorpe et al 1998). KCNN4 expression analysis in family NA showed that the R352H mutation did not impair its mRNA expression. Moreover, red cell membrane proteins involved in other RBC disorders, including AE1, ABCB6, and EPB72, were unaltered in their expression levels in family NA, consistent with an independent pathogenic

mechanism in KCNN4 mutation-associated hemolytic anemia. Moreover, apparent reductions in PIEZO1 protein abundance did not clearly cosegregate with the DHS phenotype. With this study we have expanded the cohort of DHS families with KCNN4 mutations, describing two previously undiagnosed families and one novel mutation. Future electrophysiological studies will investigate possible alterations in KCNN4 gating or ion selectivity that associated with the novel mutation V282M. Severely affected DHS patients with these KCNN4 mutations should be considered for treatment with the Gardos channel inhibitor, senicapoc (Ataga et al 2011).

The collection of new cases of DHS has allowed us to perform the molecular characterization of seven DHS patients from two unrelated families both carrying a novel in frame duplication. One proband of the two families carried also a novel missense mutation in *PIEZO1* gene. The functional study revealed the causative role of both novel mutations here described. Moreover, we demonstrated the phenotype-modifier role of the *de novo* mutation R1864H, *in cis* with the inherited duplication E2492_L2493dup on the occurrence of severe phenotype observed in the proband of family 2. This finding highlighted the importance to study the effect of multiple modifier PIEZO1 variants on the genotype-phenotype correlation, considering also that *PIEZO1* gene is a highly polymorphic *locus*. Moreover, it opens the field of study of modifier variants in other genes involved in iron metabolism and erythroid transport that could explain the variable expressivity observed in this condition.

6. CONCLUSIONS

The research effort allowed us to demonstrated the pathogenetic mechanism of FP, to find another causative gene of DHS, *KCNN4*, and finally to characterize new mutations of *PIEZO1* gene.

Our findings demonstrate that both heterozygous and homozygous missense mutations in ABCB6 lead to increased efflux of cellular K+ from HEK-293 cells, a property shared with RBCs of FP patients. Screening for the most frequently found ABCB6 variant, R276W, confirmed that patients with FP are relatively common in the blood donor population. Storage of FP blood can cause a significant increase in whole blood K+ levels, with serious clinical implications for neonates and infants receiving large-volume transfusions of whole blood. For these reasons, we endorse the proposal to conduct genetic screening for ABCB6 FP mutations among potential blood donors, especially when whole blood is needed. Finally, investigation of ABCB6 may contribute to our understanding of other pathologies of red blood cell hydration, such as sickle cell anemia.

Hyper-activation of either PIEZO1 or the Gardos channel leads to similar clinical phenotypes, strongly suggesting that both channels act together to shrink RBC volume under mechanical stress. It is likely that hyperactivity of the Gardos channel is responsible for K+ and water efflux, either because of an activating mutation in Gardos channel or because of mutations in PIEZO1 that would increase intracellular Ca2+ level and subsequently activate Gardos channel. However, PIEZO1 is more selective to K+ than it is to Ca2+ and mutations that prolong the conductive state of the channel are expected to increase the K+ leak through PIEZO1, independent of an eventual activation of the Gardos channel due to increased Ca2+ permeability. Further research on ion selectivity of mutated PIEZO1 is necessary to fully understand its involvement in red cell dehydration. Although both the PIEZO1 and Gardos channels are expressed in other tissues, dysfunction of these proteins leads to defects only in circulating cells such as RBC. This suggests that compensatory mechanisms might take place specifically in the other tissues where these proteins are expressed. Other unsolved questions are the development of iron overload and the possible link to the alteration of ionic content and the occurrence of thrombosis event after splenectomy.

7. REFERENCES

- Andolfo I, Alper SL, De Franceschi L, et al. Multiple clinical forms of dehydrated hereditary stomatocytosis arise from mutations in PIEZO1. Blood. 2013;121(19):3925-3935, S1- 12.
- Andolfo I, Alper SL, Delaunay J, et al. Missense mutations in the ABCB6 transporter cause dominant familial pseudohyperkalemia. Am J Hematol. 2013;88(1): 66-72.
- Andolfo I, Russo R, Gambale A, Iolascon A. New insights on hereditary erythrocyte membrane defects. Haematologica. 2016 Nov;101(11):1284-1294
- Andolfo I, Russo R, Manna F, et al. Functional characterization of novel ABCB6 mutations and their clinical implications in familial pseudohyperkalemia. Haematologica. 2016;101(8):909-917.
- Ataga KI, Reid M, Ballas SK, et al. Improvements in haemolysis and indicators of erythrocyte survival do not correlate with acute vaso-occlusive crises in patients with sickle cell disease: A phase III randomized, placebo-controlled, double-blind study of the Gardos channel blocker senicapoc (ICA-17043). Br J Haematol 2011;153:92–104.
- Auton A, Brooks LD, et al. 1000 Genomes Project Consortium. A global reference for human genetic variation. Nature. 2015;526(7571):68-74
- Bae C, Gnanasambandam R, Nicolai C, Sachs F, Gottlieb PA. Xerocytosis is caused by mutations that alter the kinetics of the mechanosensitive channel PIEZO1. Proc Natl Acad Sci USA. 2013;110(12):E1162-1168.
- Bagriantsev, S.N., Gracheva, E.O. & Gallagher, P.G. Piezo proteins: regulators of mechanosensation and other cellular processes. Journal of Biological Chemistry. 2014; 289:31673–31681.
- Bailey MA, Grabe M, Devor DC. Characterization of the PCMBS-dependent modification of KCa3.1 channel gating. J Gen Physiol 2010;136: 367–387.
- Bawazir WM, Flatt JF, Wallis JP, et al. Familial pseudohyperkalemia in blood donors: a novel mutation with implications for transfusion practice. Transfusion. 2014;54(12):3043-3050.
- Baz EM, Kanazi GE, Mahfouz RA, et al. An unusual case of hyperkalaemia-induced cardiac arrest in a paediatric patient during transfusion of a “fresh” 6-day-old blood unit. Transfus Med. 2002;12(6):383-386.
- Berne JD, Asensio JA, Falabella A, Gomez H. Traumatic rupture of the spleen in a patient with hereditary spherocytosis. J Trauma. 1997;42(2):323-326.
- Bianchi P, Fermo E, Vercellati C, et al. Diagnostic power of laboratory tests for hereditary spherocytosis: a comparison study in 150 patients grouped according to molecular and clinical characteristics. Haematologica. 2012;97(4):516-523.
- Bogardus HH, Maksimova YD, Forget BG, Gallagher PG. A de novo band 3 mutation in hereditary spherocytosis. Pediatr Blood Cancer. 2012;58(6):1004.
- Bolton-Maggs PH, Langer JC, Iolascon A, Tittensor P, King MJ, General Haematology Task Force of the British Committee for Standards in H.

Guidelines for the diagnosis and management of hereditary spherocytosis--2011 update. Br J Haematol. 2012;156 (1):37-49.
- Cahalan SM, Lukacs V, Ranade SS, Chien S, Bandell M, Patapoutian A. Piezo1 links mechanical forces to red blood cell volume. eLife. 2015;22;4.
- Carella M, d'Adamo AP, Grootenboer- Mignot S, et al. A second locus mapping to 2q35-36 for familial pseudohyperkalaemia. Eur J Hum Genet. 2004;12(12):1073-1076.
- Carella M, Stewart G, Ajetunmobi JF, et al. Genomewide search for dehydrated hereditary stomatocytosis (hereditary xerocytosis): mapping of locus to chromosome 16 (16q23- qter). Am J Hum Genet. 1998;63(3):810-816.
- Chen CH, Hong CL, Kau YC, et al. Fatal hyperkalemia during rapid and massive blood transfusion in a child undergoing hip surgery—a case report. Acta Anaesthesiol Sin. 1999;37(3):163-166.
- Chen K, Liu J, Heck S, Chasis JA, An X, Mohandas N. Resolving the distinct stages in erythroid differentiation based on dynamic changes in membrane protein expression during erythropoiesis. Proc Natl Acad Sci U S A. 2009;106(41):17413-17418.
- Christophersen, P. & Wulff, H. Pharmacological gating modulation of small- and intermediate-conductance Ca(2+)-activated K(+) channels (KCa2.x and KCa3.1). Channels (Austin). 2015; 9: 336–343.
- Cinar E, Zhou S, DeCourcey J, Wang Y, Waugh RE, Wan J. Piezo1 regulates mechanotransductive release of ATP from human RBCs. Proc Natl Acad Sci USA. 2015; 112(38):11783-11788.
- Coste B, Mathur J, Schmidt M, et al. Piezo1 and Piezo2 are essential components of distinct mechanically activated cation channels. Science. 2010;330(6000):55-60.
- Coste B, Murthy SE, Mathur J, et al. Piezo1 ion channel pore properties are dictated by C-terminal region. Nat Commun. 2015; 6:7223.
- Coste B, Xiao B, Santos JS, et al. Piezo proteins are pore-forming subunits of mechanically activated channels. Nature. 2012;483(7388):176-181.
- Da Costa L, Galimand J, Fenneteau O, Mohandas N. Hereditary spherocytosis, elliptocytosis, and other red cell membrane disorders. Blood reviews. 2013;27(4):167-178.
- De Franceschi L, Bosman GJ, Mohandas N. Abnormal red cell features associated with hereditary neurodegenerative disorders: the neuroacanthocytosis syndromes. Curr Opin Hematol. 2014;21(3):201-209.
- De Franceschi L, Ronzoni L, Cappellini MD, et al. K-CL co-transport plays an important role in normal and beta thalassemic erythropoiesis. Haematologica. 2007;92(10):1319-1326.
- Delaunay J. The hereditary stomatocytoses: genetic disorders of the red cell membrane permeability to monovalent cations. Semin Hematol. 2004;41(2):165-172.
- Delaunay J. The molecular basis of hereditary red cell membrane disorders. Blood Rev. 2007;21(1):1-20.

- Faucherre A, Kissa K, Nargeot J, Mangoni ME, Jopling C. Comment on: 'Homozygous knockout of the piezo1 gene in the zebrafish is not associated with anemia'. Haematologica. 2016;101(1):e38.
- Fotiou, E., Martin-Almedina, S., Simpson, M.A., et al. Novel mutations in PIEZO1 cause an autosomal recessive generalized lymphatic dysplasia with non-immune hydrops fetalis. Nature Communications. 2015. 6: 8085.
- Gallagher PG. Abnormalities of the erythrocyte membrane. Pediatr Clin North Am. 2013;60(6):1349-1362.
- Garneau L, Klein H, Parent L, Sauve R. Toward the rational design of constitutively active KCa3.1 mutant channels. Meth Enzymol 2010; 485:437–457.
- Ge J, Li W, Zhao Q, et al. Architecture of the mammalian mechanosensitive Piezo1 channel. Nature. 2015;527(7576):64-69.
- Glogowska E, Lezon-Geyda K, Maksimova Y, Schulz VP, Gallagher PG. Mutations in the Gardos channel (KCNN4) are associated with hereditary xerocytosis. Blood. 2015;126(11):1281-1284.
- Gnanasambandam, R., Bae, C., Gottlieb, P.A. Sachs, F. (2015) Ionic Selectivity and Permeation Properties of Human PIEZO1 Channels. PLoS ONE. 2015; 10:e0125503.
- Grootenboer S, Schischmanoff PO, Cynober T, et al. A genetic syndrome associating dehydrated hereditary stomatocytosis, pseudohyperkalaemia and perinatal oedema. Br J Haematol. 1998;103(2):383-386.
- Grootenboer S, Schischmanoff PO, Laurendeau I, et al. Pleiotropic syndrome of dehydrated hereditary stomatocytosis, pseudohyperkalemia, and perinatal edema maps to 16q23-q24. Blood. 2000;96(7):2599- 2605.
- Hall TL, Barnes A, Miller JR, et al. Neonatal mortality following transfusion of red cells with high plasma potassium levels. Transfusion. 1993;33(7):606-609.
- Helias V, Saison C, Ballif BA, et al. ABCB6 is dispensable for erythropoiesis and specifies the new blood group system Langereis. Nature genetics. 2012;44(2):170-173.
- Higgins, C. F. The ABC of Channel Regulation. Cell. 1995;82(5):693–669.
- Inagaki N, Gonoi T, Clement JP, et al. Reconstitution of IKATP: an inward rectifier subunit plus the sulfonylurea receptor. Science. 1995;270(5239):1166-1170. 16
- Iolascon A, De Falco L, Borgese F, et al. A novel erythroid anion exchange variant (Gly796Arg) of hereditary stomatocytosis associated with dyserythropoiesis. Haematologica. 2009;94(8):1049-1059.
- Iolascon A, Perrotta S, Stewart GW. Red blood cell membrane defects. Rev Clin Exp Hematol. 2003;7(1):22-56.
- Jamwal M, Aggarwal A, Kumar V, et al. Disease-modifying influences of coexistent G6PD-deficiency, Gilbert syndrome and deletional alpha thalassemia in hereditary spherocytosis: A report of three cases. Clin Chim Acta. 2016;458:51-54.
- Jones L, Refai Z, Linney M. An adolescent with hereditary spherocytosis who presented with splenic infarction. BMJ Case Rep. 2015;2015.

- Kim, S.E., Coste, B., Chadha, A., Cook, B., Patapoutian, A. (2012) The role of Drosophila Piezo in mechanical nociception. Nature. 2012; 483: 209–212.
- King MJ, Telfer P, MacKinnon H, et al. Using the eosin-5-maleimide binding test in the differential diagnosis of hereditary spherocytosis and hereditary pyropoikilocytosis. Cytometry B Clin Cytom. 2008;74(4):244- 250.
- Kiss K, Brozik A, Kucsma N, et al. Shifting the paradigm: the putative mitochondrial protein ABCB6 resides in the lysosomes of cells and in the plasma membrane of erythrocytes. PloS one. 2012;7(5):e37378.
- Koszarska M, Kucsma N, Kiss K, et al. Screening the expression of ABCB6 in erythrocytes reveals an unexpectedly high frequency of Lan mutations in healthy individuals. PLoS One. 2014;9(10):e111590.
- Krishnamurthy PC, Du G, Fukuda Y, et al. Identification of a mammalian mitochondrial porphyrin transporter. Nature 2006;443:586–589.Kulkeaw K, Sugiyama D. Zebrafish erythropoiesis and the utility of fish as models of anemia. Stem Cell Res Ther. 2012;3(6):55.
- Lee AC, Reduque LL, Luban NL, et al. Transfusion associated hyperkalemic cardiac arrest in pediatric patients receiving massive transfusion. Transfusion. 2014;54(1):244-254.
- Lee JH, Moon KR. Coexistence of gilbert syndrome and hereditary spherocytosis in a child presenting with extreme jaundice. Pediatr Gastroenterol Hepatol Nutr. 2014;17(4):266-269.
- Liu H, Li Y, Hung KK, Wang N, et al. Genome-wide linkage, exome sequencing and functional analyses identify ABCB6 as the pathogenic gene of dyschromatosis universalis hereditaria. PLoS One. 2014 Feb 3;9(2):e87250.
- Liu SC, Derick LH, Palek J. Visualization of the hexagonal lattice in the erythrocyte membrane skeleton. J Cell Biol. 1987;104 (3):527-536.
- Lupo F, Russo R, Iolascon A, et al. Protease inhibitors-based therapy induces acquired spherocytic-like anaemia and ineffective erythropoiesis in chronic hepatitis C virus patients. Liver Int. 2016;36(1):49-58.
- Lux SE. Anatomy of the red cell membrane skeleton: unanswered questions. Blood. 2016;127(2):187-199.
- Lux SE. Dissecting the red cell membrane skeleton. Nature. 1979;281(5731):426-429.
- Maher AD, Kuchel PW. The Gardos channel: A review of the Ca11-activated K1 channel in human erythrocytes. Int J Biochem Cell Biol 2003;35:1182–1197.
- McHugh BJ, Buttery R, Lad Y, et al. Integrin activation by Fam38A uses a novel mechanism of R-Ras targeting to the endoplasmic reticulum. J Cell Sci 2010;123:51–61.
- McHugh BJ, Murdoch A, Haslett C, Sethi T. Loss of the integrin-activating transmembrane protein Fam38A (Piezo1) promotes a switch to a reduced integrin-dependent mode of cell migration. PLoS One 2012;7:e40346.

- Mitsuhashi N, Miki T, Senbongi H, et al. MTABC3, a novel mitochondrial ATP binding cassette protein involved in iron homeostasis. J Biol Chem 2000;275: 17536–17540.
- Mohandas N, Gallagher PG. Red cell membrane: past, present, and future. Blood. 2008;112(10):3939-3948.
- Packman CH. The Clinical Pictures of Autoimmune Hemolytic Anemia. Transfus Med Hemother. 2015;42(5):317-324.
- Perrotta S, Gallagher PG, Mohandas N. Hereditary spherocytosis. Lancet. 2008;372(9647):1411-1426.
- Picard V, Proust A, Eveillard M, et al. Homozygous Southeast Asian ovalocytosis is a severe dyserythropoietic anemia associated with distal renal tubular acidosis. Blood. 2014;123(12):1963-1965.
- Ranade, S.S., Qiu, Z., Woo, S.H., Piezo1, a mechanically activated ion channel, is required for vascular development in mice. Proc Natl Acad Sci U S A. 2014; 111:10347–10352.
- Rapetti-Mauss R, Lacoste C, Picard V, et al. A mutation in the Gardos channel is associated with hereditary xerocytosis. Blood. 2015;126(11):1273-1280.
- Shmukler BE, Huston NC, Thon JN, et al. Homozygous knockout of the piezo1 gene in the zebrafish is not associated with anemia. Haematologica. 2015;100(12):e483-485.
- Shmukler BE, Lawson ND, Paw BH, Alper SL. Authors' response to "Comment on: 'Homozygous knockout of the piezo1 gene in the zebrafish is not associated with anemia'". Haematologica. 2016;101(1):e39.
- Smith HM, Farrow SJ, Ackerman JD, et al. Cardiac arrests associated with hyperkalemia during red blood cell transfusion: a case series. Anesth Analg. 2008;106(4):1062-1069.
- Stewart GW, Corrall RJ, Fyffe JA, Stockdill G, Strong JA. Familial pseudohyperkalaemia. A new syndrome. Lancet. 1979;2(8135):175-177.
- Suzuki Y, Shichishima T, Mukae M, et al. Splenic infarction after Epstein-Barr virus infection in a patient with hereditary spherocytosis. Int J Hematol. 2007;85(5):380-383.
- Syfuss PY, Ciupea A, Brahimi S, et al. Mild dehydrated hereditary stomatocytosis revealed by marked hepatosiderosis. Clin Lab Haematol. 2006;28(4):270-274.
- Szakacs G, Annereau JP, Lababidi S, et al. Predicting drug sensitivity and resistance: Profiling ABC transporter genes in cancer cells. Cancer Cell 2004;6:129–137.
- Thomas, S.L., Bouyer, G., Cueff, A., Egee, S., Glogowska, E. & Ollivaux, C. Ion channels in human red blood cell membrane: actors or relics? Blood Cells, Molecules, & Diseases. 2011; 46: 261–265.
- Tsuchida M, Emi Y, Kida Y, et al. Human ABC transporter isoform B6 (ABCB6) localizes primarily in the Golgi apparatus. Biochem Biophys Res Commun 2008;369:369–375.

- Ulrich DL, Lynch J, Wang Y, et al. ATP-dependent mitochondrial porphyrin importer ABCB6 protects against phenylhydrazine toxicity. J Biol Chem 2012;287:12679–12690.
- Vandorpe DH, Shmukler BE, Jiang L, et al. cDNA cloning and functional characterization of the mouse Ca2+-gated K1 channel, mIK1. Roles in regulatory volume decrease and erythroid differentiation. J Biol Chem 1998;273: 21542–21553.
- Vantyghem MC, Dagher G, Doise B, et al. Pseudo-hyperkalemia. Apropos of a familial case. Ann Endocrinol (Paris). 1991;52(2):104–108.
- Wang L, He F, Bu J, et al. ABCB6 mutations cause ocular coloboma. Am J Hum Genet 2012;90:40–48.
- Weber GJ, Choe SE, Dooley KA, et al. Mutant-specific gene programs in the zebrafish. Blood 2005;106:521–530
- Welsh MJ, Anderson MP, Rich DP, et al. Cystic fibrosis transmembrane conductance regulator: a chloride channel with novel regulation. Neuron. 1992;8(5):821-829.
- Zarychanski R, Schulz VP, Houston BL, et al. Mutations in the mechanotransduction protein PIEZO1 are associated with hereditary xerocytosis. Blood. 2012;120(9):1908-1915.
- Zutz A, Gompf S, Schagger H, et al. Mitochondrial ABC proteins in health and disease. Biochim Biophys Acta. 2009;1787:681–690.

8. LIST OF PUBLICATIONS OF THE STUDENT RELATED TO THE THESIS

- **Andolfo I**, Russo R, Gambale A, Iolascon A. New insights on hereditary erythrocyte membrane defects. Haematologica. 2016 Nov;101(11):1284-1294. Review. PMID: 27756835

- Russo R, **Andolfo I,** Manna F, De Rosa G, De Falco L, Gambale A, Bruno M, Mattè A, Ricchi P, Girelli D, De Franceschi L, Iolascon A. Increased levels of ERFE-encoding FAM132B in patients with congenital dyserythropoietic anemia type II. Blood. 2016 Aug 18. PMID: 27540014

- **Andolfo I**, Russo R, Manna F, De Rosa G, Gambale A, Zouwail S, Detta N, Pardo CL, Alper SL, Brugnara C, Sharma AK, De Franceschi L, Iolascon A. Functional characterization of novel ABCB6 mutations and their clinical implications in familial pseudohyperkalemia. Haematologica. 2016 Aug;101(8):909-17. PMID: 27151991

- Russo R, **Andolfo I**, Iolascon A. Next generation research and therapy in red blood cell diseases. Haematologica. 2016 May;101(5):515-7. PMID: 27132276 .

- The European Hematology Association Roadmap for European Hematology Research: a consensus document. Engert A, Balduini C, Brand A, Coiffier B, Cordonnier C, Döhner H, de Wit TD, Eichinger S, Fibbe W, Green T, de Haas F, Iolascon A, Jaffredo T, Rodeghiero F, Salles G, Schuringa JJ, André M, Andre-Schmutz I, Bacigalupo A, Bochud PY, Boer Md, Bonini C, Camaschella C, Cant A, Cappellini MD, Cazzola M, Celso CL, Dimopoulos M, Douay L, Dzierzak E, Einsele H, Ferreri A, De Franceschi L, Gaulard P, Gottgens B, Greinacher A, Greinacher A, Gresele P, Gribben J, de Haan G, Hansen JB, Hochhaus A, Kadir R, Kaveri S, Kouskoff V, Kühne T, Kyrle P, Ljungman P, Maschmeyer G, Méndez-Ferrer S, Milsom M, Mummery C, Ossenkoppele G, Pecci A, Peyvandi F, Philipsen S, Reitsma P, Ribera JM, Risitano A, Rivella S, Ruf W, Schroeder T, Scully M, Socie G, Staal F, Stanworth S, Stauder R, Stilgenbauer S, Tamary H, Theilgaard-Mönch K, Thein SL, Tilly H, Trneny M, Vainchenker W, Vannucchi AM, Viscoli C, Vrielink H, Zaaijer H, Zanella A, Zolla L, Zwaginga JJ, Martinez PA, van den Akker E, Allard S, Anagnou N, **Andolfo I,** et al. EHA Roadmap for European Hematology Research. Haematologica. 2016 Feb;101(2):115-208.PMID: 26819058

- Gambale A, Iolascon A, **Andolfo I**, Russo R. Diagnosis and management of congenital dyserythropoietic anemias. Expert Rev Hematol. 2016 Jan 6:1-14.

- **Andolfo I**, Russo R, Manna F, Shmukler BE, Gambale A, Vitiello G, De Rosa G, Brugnara C, Alper SL, Snyder LM, Iolascon A. Novel Gardos channel mutations linked to dehydrated hereditary stomatocytosis (xerocytosis). Am J Hematol. 2015 Oct;90(10):921-6.

- Kalish BT, Matte A, **Andolfo I**, Iolascon A, Weinberg O, Ghigo A, Cimino J, Siciliano A, Hirsch E, Federti E, Puder M, Brugnara C, De Franceschi L. Dietary ω-3 fatty acids protect against vasculopathy in a transgenic mouse model of sickle cell disease. Haematologica. 2015 Jul;100(7):870-80.

- Iolascon A, **Andolfo I**, Russo R. Red cells in post-genomic era: impact of personalized medicine in the treatment of anemias. Haematologica. 2015

Jan;100(1):3-6.

- Russo R, Gambale A, Langella C, **Andolfo I**, Unal S, Iolascon A. Retrospective cohort study of 205 cases with congenital dyserythropoietic anemia type II: definition of clinical and molecular spectrum and identification of new diagnostic scores. Am J Hematol. 2014 Oct;89(10):E169-75.

- Archer NM, Shmukler BE, **Andolfo I**, Vandorpe DH, Gnanasambandam R, Higgins JM, Rivera A, Fleming MD, Sachs F, Gottlieb PA, Iolascon A, Brugnara C, Alper SL, Nathan DG. Hereditary xerocytosis revisited. Am J Hematol. 2014 Dec;89(12):1142-6.